Clim. Past, 9, 2173–2193, 2013
www.clim-past.net/9/2173/2013/
doi:10.5194/cp-9-2173-2013

Climate of the Past
Open Access

Can we determine what controls the spatio-temporal distribution of d-excess and ^{17}O-excess in precipitation using the LMDZ general circulation model?

C. Risi[1], A. Landais[2], R. Winkler[2], and F. Vimeux[2,3]

[1]Laboratoire de Météorologie Dynamique UMR8539, IPSL/CNRS/UPMC, 4, place Jussieu, 75252 Paris Cedex 05, France
[2]Institut Pierre Simon Laplace (IPSL), Laboratoire des Sciences de Climat et de l'Environnement (LSCE), UMR8212 (CEA-CNRS-UVSQ), CE Saclay, Orme des Merisiers, Bât. 701, 91191 Gif-sur-Yvette, Cedex, France.
[3]Institut de Recherche pour le Développement (IRD), Laboratoire HydroSciences Montpellier (HSM), UMR5569 (CNRS-IRD-UM1-UM2), Montpellier, France

Correspondence to: C. Risi (camille.risi@lmd.jussieu.fr)

Received: 17 September 2012 – Published in Clim. Past Discuss.: 8 November 2012
Revised: 12 July 2013 – Accepted: 7 August 2013 – Published: 16 September 2013

Abstract. Combined measurements of the $H_2^{18}O$ and HDO isotopic ratios in precipitation, leading to second-order parameter D-excess, have provided additional constraints on past climates compared to the $H_2^{18}O$ isotopic ratio alone. More recently, measurements of $H_2^{17}O$ have led to another second-order parameter: ^{17}O-excess. Recent studies suggest that ^{17}O-excess in polar ice may provide information on evaporative conditions at the moisture source. However, the processes controlling the spatio-temporal distribution of ^{17}O-excess are still far from being fully understood.

We use the isotopic general circulation model (GCM) LMDZ to better understand what controls d-excess and ^{17}O-excess in precipitation at present-day (PD) and during the last glacial maximum (LGM). The simulation of D-excess and ^{17}O-excess is evaluated against measurements in meteoric water, water vapor and polar ice cores. A set of sensitivity tests and diagnostics are used to quantify the relative effects of evaporative conditions (sea surface temperature and relative humidity), Rayleigh distillation, mixing between vapors from different origins, precipitation re-evaporation and supersaturation during condensation at low temperature.

In LMDZ, simulations suggest that in the tropics convective processes and rain re-evaporation are important controls on precipitation D-excess and ^{17}O-excess. In higher latitudes, the effect of distillation, mixing between vapors from different origins and supersaturation are the most important controls. For example, the lower D-excess and ^{17}O-excess at LGM simulated at LGM are mainly due to the supersaturation effect. The effect of supersaturation is however very sensitive to a parameter whose tuning would require more measurements and laboratory experiments. Evaporative conditions had previously been suggested to be key controlling factors of d-excess and ^{17}O-excess, but LMDZ underestimates their role. More generally, some shortcomings in the simulation of ^{17}O-excess by LMDZ suggest that general circulation models are not yet the perfect tool to quantify with confidence all processes controlling ^{17}O-excess.

1 Introduction

Water-stable isotopic measurements in ice cores have long been used to reconstruct past climates. In particular, the $H_2^{18}O$ and HDO isotopic ratio (expressed, respectively through δD and δ^{18}O) in polar ice cores have long been used as a proxy of past polar temperature (Johnsen et al., 1972; Lorius et al., 1979; Jouzel, 2003). Combined measurements of $H_2^{18}O$ and HDO isotopic ratio in precipitation, leading to second-order parameter D-excess (d-excess $= \delta D - 8\delta^{18}O$, Dansgaard, 1964), have provided additional constraints on past climates compared to the $H_2^{18}O$ or HDO ratios alone. Its interpretation is however more complex. First interpreted as a tracer of relative humidity conditions at the moisture source (Jouzel et al., 1982), it was later interpreted in terms of the

temperature at the moisture source or of shifts in moisture origin (Stenni et al., 2001; Vimeux et al., 2002; Masson-Delmotte et al., 2005). It is also impacted by mixing along trajectories (Hendricks et al., 2000; Sodemann et al., 2008) and local temperature (Masson-Delmotte et al., 2008). In models, its representation is very sensitive to a poorly constrained empirical parameter determining the supersaturation in polar clouds (Jouzel and Merlivat, 1984).

More recently, measurements of $H_2^{17}O$ have led to the definition of another second-order parameter: ^{17}O-excess=$\left(\ln(\delta^{17}O/1000+1)-0.528\times\ln(\delta^{18}O/1000+1)\right)$ (Landais et al., 2006). Since magnitudes of ^{17}O-excess are very small, they are multiplied by 10^6 and expressed in per meg (Landais et al., 2008). Recent studies suggest that ^{17}O-excess may provide information on evaporative conditions at the source of moisture (Barkan and Luz, 2007; Landais et al., 2008; Risi et al., 2010c; Uemura et al., 2010). Potentially, the combination of δ^{18}O, d-excess and ^{17}O-excess may thus enable us to describe more comprehensively past climate changes, including local temperature, moisture origin and conditions at the moisture source. However, processes controlling ^{17}O-excess appear even more complex than those controlling d-excess. As d-excess, ^{17}O-excess is strongly sensitive to the empirical parameter determining the supersaturation in polar clouds (Winkler et al., 2012; Landais et al., 2012a,b). In addition, its logarithmic definition makes it very sensitive to mixing between vapors of different origins: for example, mixing vapors of same ^{17}O-excess and different δ^{18}O leads to lower ^{17}O-excess in the mixture (Risi et al., 2010c). In Central Antarctica, ^{17}O-excess may also be affected by stratospheric intrusions (Winkler et al., 2013). Indeed, the ^{17}O-excess in the stratospheric vapor is so high (of the order of 3000 permeg, Franz and Roeckmann, 2005; Zahn et al., 2006) relatively to that in the tropospheric vapor (a few tens of per meg maximum) that even a small flux of stratospheric vapor into the troposphere may affect significantly the tropospheric ^{17}O-excess.

This paper aims at better understanding what processes controls the spatio-temporal distribution of d-excess and ^{17}O-excess, and what processes make δ^{18}O, d-excess and ^{17}O-excess complementary tracers. These questions have so far been addressed using simple models: Rayleigh distillation models (Landais et al., 2008, 2012b) which can be coupled to a back-trajectory analysis (Winkler et al., 2012), a single column model (Risi et al., 2010c) or a bulk re-evaporation model (Landais et al., 2010). To take into account a broader range of processes controlling the water isotopic composition, we use the isotope-enabled general circulation model (GCM) LMDZ (Risi et al., 2010b), in which we have implemented $H_2^{17}O$. The added value of GCMs compared to simpler models is that they represent the integrated effects, along air mass trajectories, of boundary layer and convective processes, cloud and precipitation physics, evaporative recycling and mixing between different air masses. To investigate the effect of this combination of processes, isotopic GCMs are invaluable. For example, isotopic GCM simulations have been exploited to understand how δ^{18}O and d-excess relate to the origin of water vapor (e.g. Delaygue, 2000; Werner et al., 2001; Noone, 2008; Lee et al., 2008; Masson-Delmotte et al., 2011). The drawback of these GCM studies is however the difficulty of GCMs to simulate some aspects of observed d-excess variability. For example, simulated daily d-excess variations in the water vapor or in the precipitation are too flat (Risi et al., 2010b; Steen-Larsen et al., 2013) and simulated d-excess variations at the paleo-climatic scale are always of opposite sign compared to δ^{18}O even when observed variations are of the same sign (Werner et al., 2001; Noone, 2008). This difficulty reflects the complexity of the d-excess variable and our lack of understanding of its major controlling factors. This difficulty is expected to be even more severe for ^{17}O-excess.

To our knowledge, this is the first time ^{17}O-excess simulations with a GCM are being documented. The first goal of this paper is thus to document the performance of GCMs in capturing observed spatio-temporal variations in ^{17}O-excess. This allows us to better assess the feasibility of using a GCM to investigate what controls ^{17}O-excess. For features that the model can capture well, we use the GCM to disentangle the different processes controlling ^{17}O-excess and contrast them with processes controlling δ^{18}O and d-excess. For features that the model cannot capture well, we suggest possible causes of mismatches. As a first study of ^{17}O-excess in a GCM, we focus on latitudinal gradients, seasonal variability and difference between the Last Glacial Maximum (LGM) and present-day (PD).

In Sect. 2, we describe the model simulations, data sets and methodology. In Sect. 3, we evaluate the model isotopic simulations. In Sect. 4, we quantify the factors controlling the δ^{18}O, d-excess and ^{17}O-excess distributions simulated by LMDZ and discuss implications for the factors in the real world. In Sect. 5, we summarize our results and present perspectives for future work.

2 Model simulations, data sets and methodology

2.1 The LMDZ4 model and isotopic implementation

LMDZ4 (Hourdin et al., 2006) is the atmospheric component of the Institut Pierre-Simon Laplace coupled model (IPSL-CM4, Marti et al., 2005) used in CMIP3 (Coupled Model Intercomparison Project, Meehl et al., 2007). It is used here with a resolution of 2.5° in latitude, 3.75° in longitude and 19 vertical levels. The physical package includes the Emanuel convective scheme (Emanuel, 1991; Emanuel and Zivkovic-Rothman, 1999), coupled to a statistical cloud scheme (Bony and Emanuel, 2001) which diagnoses convective cloud fraction from a radiative point of view. Precipitation can be created either by the convective scheme or by a large-scale

condensation scheme. The large-scale condensation scheme is also based on a statistical cloud scheme (Letreut and Li, 1991). The impact of tuning parameters in this statistical cloud scheme on water isotopic compositions are limited to the upper troposphere (Risi et al., 2012). Water vapor and condensate are advected using a second-order monotonic finite volume advection scheme (Van Leer, 1977; Hourdin and Armengaud, 1999).

The isotopic version of LMDZ is described in detail in Risi et al. (2010b). Equilibrium fractionation coefficients between vapor and liquid water or ice are calculated after Merlivat and Nief (1967), Majoube (1971a) and Majoube (1971b). The isotopic composition of the ocean surface evaporation flux is calculated following Craig and Gordon (1965). We take into account kinetic effects during the evaporation from the sea surface following Merlivat and Jouzel (1979) and during snow formation following Jouzel and Merlivat (1984), with the supersaturation parameter λ set to 0.004 to optimize the simulation of d-excess over Antarctica (Risi et al., 2010b). This λ value is consistent with that found to optimize the simulation of both d-excess and ^{17}O-excess in both Antarctica and Greenland in simpler models (Landais et al., 2012a,b). We make the simplifying assumption that over land, all evapotranspiration occurs as transpiration (e.g. Hoffmann et al., 1998), which is non-fractionating (Washburn and Smith, 1934; Barnes and Allison, 1988). Specifically for $H_2^{17}O$, equilibrium fractionation coefficients are equal those for $H_2^{18}O$ at the power 0.529 (Van Hook, 1968; Barkan and Luz, 2005; Landais et al., 2012b). The diffusivity of $H_2^{17}O$ relatively to that of $H_2^{16}O$ is assumed to be that for $H_2^{18}O$ at the power 0.518 (Barkan and Luz, 2007).

We do not consider the effect of methane oxidation on the stratospheric water isotopic composition (Johnson et al., 2001; Zahn et al., 2006). This is a reasonable approximation since we focus on the isotopic composition of the precipitation and of low-level vapor. It has been shown that in Central Antarctica, stratospheric intrusions may play a role in the inter-annual variability of Vostok precipitation ^{17}O-excess, but the role of these intrusions in the spatial and seasonal distribution of ^{17}O-excess and in its LGM-to-present variation is unclear.

The implementation of stable water isotopes in the convective scheme has been extensively described in Bony et al. (2008). In convective updrafts, condensation is assumed to be a closed process (i.e. vapor-condensate equilibrium) for the liquid phase (above -40°C) and an open process (i.e. Rayleigh distillation) for the ice phase (below 0°C). We pay particular attention to the representation of the re-evaporation and diffusive exchanges as the rain falls, which is significantly more detailed compared to other GCMs: at each time step and at each level, the model takes into account the evolution of the compositions of both the rain and the surrounding vapor as the rain drops re-evaporate (Bony et al., 2008), whereas most GCMs take into account the evolution of the composition in the rain only. The relative proportion of evaporative enrichment and diffusive equilibration is calculated at each level depending on surrounding relative humidity following Stewart (1975). The surrounding relative humidity is calculated as $\phi + (1-\phi) \cdot h_{\mathrm{ddft}}$ with h_{ddft} being the relative humidity in the environment of the rain drops, i.e. in the unsaturated downdraft that collects the precipitation for convective precipitation, or in the large-scale environment for large-scale precipitation. The parameter ϕ was set to 0.9 to optimize the simulation of δ^{18}O and d-excess in tropical rainfall and their relationship with precipitation rate (Risi et al., 2010b), although $\phi = 0.8$ is in better agreement with some ^{17}O-excess data (Landais et al., 2010). When the relative humidity is 100 % we simply assume total reequilibration between raindrops and vapor, contrary to Stewart (1975) and Lee and Fung (2008), who take into account the raindrop size distribution in this particular case. To calculate fractionation coefficients, the temperature at each level in the environment of the rain drops is used, i.e. in the unsaturated downdraft for convective precipitation or in the large-scale environment for large-scale precipitation.

Our calculation of isotopic exchanges during rain re-evaporation involves in the general case the numerical solution of an integral (Bony et al., 2008). The number of iterations used in this solution was chosen to be sufficient to accurately predict δ^{18}O and d-excess, but was found to be insufficient to predict ^{17}O-excess. The number of iterations was thus multiplied by 2, which makes the simulation with $H_2^{17}O$ computationally slower than usual.

2.2 Model simulations

Due to computational limitations, all simulations are short (2–3 yr) but use as initial states outputs of simulations that have already been equilibrated for several years for all isotopes.

To compare with data sets, LMDZ is forced by observed sea surface temperatures (SST) and sea ice following the AMIP (Atmospheric Model Inter-comparison Project) protocol (Gates, 1992) for the year 2005–2006. The year 2005–2006 was chosen to allow daily collocation with the vapor data set of Uemura et al. (2010). Horizontal winds at each vertical level are nudged by ECMWF reanalyses (Uppala et al., 2005) as detailed in Risi et al. (2010b). This ensures a realistic large-scale circulation. When comparing with the other data sets, some of the model-data difference could be attributed to the differences in the meteorological conditions between 2005–2006 and the year of the measurement. Ideally, the full period 2000–2010 should have been simulated and outputs should have been collocated with each measurement for a perfectly rigorous comparison. However, for the first GCM evaluation for ^{17}O-excess, we focus on broad latitudinal gradients and seasonal variations that are robust with respect to inter-annual variability.

To investigate controls at paleo-timescales, we focus on the LGM period for which a large number of paleo-climate proxies are available (e.g. Farrera et al., 1999; Bartlein et al., 2010) and the forcing is relatively well-known (Braconnot et al., 2007) and strong. For the PD control simulation, LMDZ is run without nudging and forced by climatological AMIP SSTs averaged over 1979–2007. For the LGM simulation, the PMIP1 protocol is applied (Joussaume and Taylor, 1995). LMDZ is forced by SSTs and sea ice from the LongRange Investigation, Mapping, and Prediction (CLIMAP, CLIMAP, 1981) forcing. Orbital parameters and greenhouse gas concentrations are also set to their LGM values. ICE-5G ice sheet conditions are applied (Peltier, 1994). This simulation is described in Risi et al. (2010b). We use CLIMAP rather than the SSTs simulated by a coupled model (as in the PMIP2 protocol, Braconnot et al., 2007), because the SSTs and sea ice simulated by the IPSL model at LGM are unrealistically warm in the Southern Ocean (Risi et al., 2010b). As a consequence, evaporative recycling over high latitude oceans is too strong and δ^{18}O is unrealistically enriched at LGM (though d-excess is in slightly better agreement with observations) (Risi et al., 2010b). We are aware of the caveats of the CLIMAP forcing. In particular, the warm tropical SSTs and the extensive sea ice of the CLIMAP reconstruction have been questioned (MARGO project members, 2009). However, since our LGM evaluation will focus on Antarctica, where most of the ^{17}O-excess so far have been available for LGM, we prefer the caveats of CLIMAP than those of the IPSL model.

2.3 Data sets for model evaluation

To evaluate the present-day nudged simulation of δ^{18}O and d-excess, we use the GNIP (Global Network of Isotopes in Precipitation) data set (Rozanski et al., 1993) as is done in all basic isotopic modelling publications (Hoffmann et al., 1998; Risi et al., 2010b). This data set was complemented with Antarctica (Masson-Delmotte et al., 2008) and Greenland (V. Masson-Delmotte, personal communication, 2008) data and was regridded on the LMDZ grid by attributing to each LMDZ grid the average of all measurements falling into this grid.

For ^{17}O-excess, we use a set of meteoric water measurements compiled by Luz and Barkan (2010). This includes measurements in precipitation, snow, rivers and lakes (Table 1). We compare observed composition in the precipitation and in the snow to the simulated composition in the precipitation for the particular month of sampling. For the snow, we neglect post-depositional effects (e.g. Taylor and Renshaw, 2001; Gurney and Lawrence, 2004; Ekaykin et al., 2009; Lee et al., 2010). This is a reasonable assumption since seasonal cycles of δ^{18}O, d-excess and ^{17}O-excess measured in shallow cores compare well with those measured directly in the precipitation (Landais et al., 2012b). We compare observed composition in river water to the simulated annual-mean composition in the precipitation. In reality, river water composition integrates precipitation water over the previous months and over the entire watershed (Kendall and Coplen, 2001). It is additionally affected by evaporative enrichment (Gibson et al., 2005; Risi, 2009) and by temporal variations in drainage and runoff (Dutton et al., 2005). Coupling LMDZ with the land surface model ORCHIDEE (Krinner et al., 2005), equipped with a routing scheme (Polcher, 2003) and enabled with water isotopes (Risi, 2009), would be necessary to rigorously compare the model to river observations. This is beyond the scope of this paper, and this is why here we simply assume that river water is representative of the annual-mean precipitation. This assumption is justified by the fact that the isotopic seasonality in river water is usually strongly dampened relatively to that in the precipitation (Kendall and Coplen, 2001).

We add to this set some ^{17}O-excess measurements made at LSCE (Table 2): monthly-mean precipitation in the Zongo Valley in Bolivia (Vimeux et al., 2005, unpublished for d-excess and ^{17}O-excess), in Niamey (Niger, Landais et al., 2010), in NEEM (Greenland, Landais et al., 2012b) and in Vostok (Antarctica, Winkler et al., 2012). In Vostok the flow is taken into account in the age scale, though this has little impact on the last glacial–interglacial transition. We also add δ^{18}O, d-excess and ^{17}O-excess measurements along an Antarctica transect (Landais et al., 2008). To evaluate the composition of the water vapor, we use the δ^{18}O, d-excess and ^{17}O-excess measurements made during Southern Ocean cruises in 2005–2006 (Uemura et al., 2008, 2010). Finally, we use the isotopic composition measured from PD to LGM in several Antarctica ice cores: Vostok (Landais et al., 2008), Taylor Dome and Dome C (Winkler et al., 2012) (Table 3). The precision of these measurements is about 5 per meg (Landais et al., 2006).

Although ^{17}O-excess measurements are now calibrated with respect to two international standards (Schoenemann et al., 2013), there are calibration issues affecting absolute measurements of ^{17}O-excess (Winkler et al., 2012; Landais et al., 2012a). In particular, there are ^{17}O-excess calibration uncertainties for large δ^{18}O variations. This effect leads to an uncertainty of 20 per meg for δ^{18}O variations of 50 ‰. Such an uncertainty is beyond measurement precision only for δ^{18}O variations larger than 12.5 ‰. Therefore, there is some uncertainty in the latitudinal variations of ^{17}O-excess through Antarctica, where δ^{18}O strongly varies. This calls for caution when interpreting ^{17}O-excess results. In contrast, other spatial patterns as well as seasonal and LGM-PD variations, which are characterized by smaller δ^{18}O variations, are not affected by this problem. For example, ^{17}O-excess variations associated with the seasonal cycle or with the last deglaciation are very similar when measured in different laboratories (Winkler et al., 2012; Landais et al., 2012a).

Table 1. Precipitation ^{17}O-excess simulated by LMDZ, compared to data from (Luz and Barkan, 2010) collected in precipitation or rivers. We did not select lakes, caves or ponds in order to avoid samples affected by re-evaporation after rainfall. Based on land surface isotopic modelling (e.g. Fekete et al., 2006; Risi, 2009) and observations (Kendall and Coplen, 2001), we assume that river water is close to annual-mean precipitation. For rivers, we thus compare with annual mean simulated precipitation composition. When several samples are taken at the same location in the same season, we present averages.

Location	Sample type	Month	Latitude	Longitude	^{17}O-excess obs	^{17}O-excess LMDZ
Vienna, Austria	river	April	48.23	16.33	18	16.9
Yang Shou, China	river	October	24.77	110.5	52	16.5
Montenegro	snow	June	42.9	19.3	−12	31.0
Altenahr, Germany	river	August	50.52	6.99	27	24.9
Köln, Germany	river	August	50.96	6.94	16	22.4
Bacharach, Germany	river	August	50.06	7.78	23	24.9
Heidelberg, Germany	river	August	49.4	8.73	21	24.9
New Delhi, India	rain	annual	28.58	77.20	22	12.8
Ahmedabad, India	rain	annual	23.00	72.67	20	6.3
Kozhikode, India	rain	annual	11.25	75.72	20	23.5
Borneo, Indonesia	rain	March	1.00	114.00	49	25.2
Borneo, Indonesia	rain	June–August	1.00	114.00	53.5	22.3
Borneo, Indonesia	rain	November	1.00	114.00	59	25.9
Jerusalem, Israel	rain	annual	31.78	35.20	35	no rain
Jerusalem, Israel	rain	annual	31.78	35.20	35	no rain
Jerusalem, Israel	spring	February	31.78	35.20	51	no rain
Israel	river	July	33.23	35.61	55	34.0
Israel	river	July	33.23	35.63	53	28.6
Israel	river	July	32.88	35.61	36	no rain
New Zealand	river	February	−41	172	47	21.7
New Zealand	river	February	−41	172	56	21.7
St. Petersburg, Russia	river	May	42.90	19.29	40	29.0
Piermont, USA	river	August	43.97	−72.07	15	19.7
Tilton, USA	river	August	43.44	−71.59	20	19.7
Charvak, Uzbekistan	river	May	41.62	69.95	35	24.4
Edmonton, Canada	snow	December–January	53.5	−113.5	39.5	17.2
Triel, France	river	October	48.98	2.00	22	16.6

2.4 Methodology to quantify isotopic controls

Precipitation δ^{18}O, d-excess and ^{17}O-excess are decomposed into several contributions. For simplicity, we present here the method for decomposing the isotopic ratio R for any of the three heavy isotopic species (HDO, $H_2^{18}O$, $H_2^{17}O$), but the same equations apply for δ^{18}O, d-excess and ^{17}O-excess.

Precipitation composition is first decomposed into two terms:

$$R_p = R_v + \left(R_p - R_v\right).$$

The first term, R_v, is the vapor composition. It results from all processes affecting the isotopic composition of the vapor upstream air mass trajectories. The second term is the precipitation-vapor difference. This reflects local condensation and post-condensation processes, since precipitation is produced and falls locally. In the tropics, where the precipitation is liquid, $R_p - R_v$ will mainly reflect rain re-evaporation and vapor–liquid exchanges during the rainfall. At high latitudes, precipitation is solid. The diffusion of water molecules in ice is too low to allow for isotopic exchanges during the fall of snow (Jouzel, 1986). Therefore, $R_p - R_v$ will rather reflect the condensation altitude, temperature and rate. It can also depend on the vertical gradient of water vapor isotopic composition between the surface and the condensation altitude.

Then, several sensitivity tests are used to understand what controls the vapor composition R_v. Since ^{17}O-excess has been shown to be affected by evaporative conditions at the moisture source and to be sensitive to kinetic fractionation during ice condensation, we quantify preferentially these two kinds of effects. To quantify the effect of evaporative conditions, we make additional simulations in which the sea surface temperature (SST) or the relative humidity normalized by the surface temperature (RH_s) during the calculation of isotopic fractionation at ocean evaporation are fixed. This allows us to quantify the direct effect of SST and RH_s at the moisture source without changing anything

Table 2. Precipitation ^{17}O-excess simulated by LMDZ, compared to various additional measurements done at LSCE.

location	sample type	month	lat	lon	reference	^{17}O-excess obs (per meg)	^{17}O-excess LMDZ (per meg)
Zongo, Bolivia	rain	June–August	−16.15	−67.10	Vimeux et al. (2005), unp. results	15.7	21.4
Zongo, Bolivia	rain	December–February	−16.15	−67.10	Vimeux et al. (2005), unp. results	38	21
Niamey, Niger	rain	June−15 July	13.52	2.09	Risi et al. (2008b); Landais et al. (2010)	−10	8
Niamey, Niger	rain	15 July–October	13.52	2.09	Risi et al. (2008b); Landais et al. (2010)	20	15
Dome F, Antarctica	snow	annual	−77.32	39.70	Luz and Barkan (2010)	1	10.1
Vostok, Antarctica	snow	annual	−78.45	106.85	Landais et al. (2008)	3.5	−29.9
Vostok, Antarctica	snow	December–February	−78.45	106.85	Winkler et al. (2012)	18.5	−11.8
Vostok, Antarctica	snow	June–August	−78.45	106.85	Winkler et al. (2012)	−6.4	−33.2
NEEM, Greenland	snow	annual	77.5	−50.9	Landais et al. (2012b)	50	11.1
NEEM, Greenland	snow	December–February	77.5	−50.9	Landais et al. (2012b)	58.1	29.2
NEEM, Greenland	snow	June–August	77.5	−50.9	Landais et al. (2012b)	64.9	0.6
Dome C	snow	annual	−75.4	123.14	Winkler et al. (2012)	18	−9
Taylor	snow	annual	−77.28	158.26	Winkler et al. (2012)	8.9	4.1
Antarctica transect	snow	annual	−75.6 to −74.4	124.4 to 160.7	Landais et al. (2008)	30 to 59	−22 to −14

in the dynamics or in the hydrological cycle of the simulation. We call RH_scste the simulation in which the RH_s is set to 60 % during the calculation of isotopic fractionation at ocean evaporation. The effect of RH_s at the source is thus $\Delta R_{RH_s} = R_{v,control} - R_{v,RH_s cste}$. We call RH_sSSTcste the simulation in which the SST is set to 15 °C and the RH_s is set to 60 % during the calculation of isotopic fractionation at ocean evaporation. The effect of SST at the source is thus $\Delta R_{SST} = R_{v,RH_s cste} - R_{v,RH_s SSTcste}$.

To quantify kinetic fractionation during ice condensation, we perform an additional simulation (called nokin) in which this fractionation is turned off, i.e. λ is set to 0. The effect of kinetic fractionation during ice condensation is thus $\Delta R_{kin} = R_{v,control} - R_{v,nokin}$.

Assuming that all processes add up linearly, we can thus decompose R_v into four terms:

$$R_{v,control} = \left(R_{v,RH_s SSTcste} - \Delta R_{kin}\right) + \Delta R_{kin} + \Delta R_{SST} + \Delta R_{RH_s} \quad (1)$$

The first term on the right-hand side represents all the processes other than evaporative conditions and kinetic fractionation during ice condensation. In the tropics, this may represent for example convective mixing by unsaturated downdrafts (Risi et al., 2008a, more details in Sect. 4.3.1). In higher latitudes, this represents Rayleigh distillation along trajectories and mixing between vapor from different air masses. Note that the assumption that all processes add up linearly is valid for δ^{18}O and for ^{17}O-excess, but may lead to uncertainties of up to 1 ‰ for d-excess in very cold regions (Supplement). In the remaining of the paper, we will focus on d-excess variations larger than this uncertainty.

3 Model evaluation

We first evaluate the simulation of the triple isotopic composition in the water vapor, and then in the precipitation.

3.1 Water vapor isotopic composition

Few observations are available for ^{17}O-excess in the water vapor. We compare LMDZ with water vapor isotopic composition measured in the near-surface vapor along Southern Ocean transects (Uemura et al., 2008, 2010). When going poleward, observed δ^{18}O decreases consistently with the distillation of air masses (Fig. 1a, red). At the same time, d-excess and ^{17}O-excess decrease (Fig. 1b, c). This is consistent with the effect of evaporative conditions on d-excess and ^{17}O-excess (Vimeux et al., 2001a; Landais et al., 2008; Risi et al., 2010c). The RH_s increases poleward (Fig. 1d) while the SST decreases. Both RH_s and SST effects contribute to the poleward decrease of d-excess and ^{17}O-excess (Appendix A).

The Merlivat and Jouzel (1979) closure equation (Appendix A) captures the poleward decrease in d-excess and

Table 3. LGM minus present-day difference in precipitation $\delta^{18}O$, d-excess and ^{17}O-excess in Antarctica observed in ice cores and simulated by LMDZ.

	Latitude	Longitude	$\delta^{18}O$ obs (‰) (‰)	d-excess obs (per meg)	^{17}O-excess obs	$\delta^{18}O$ LMDZ (‰)	d-excess LMDZ (‰)	^{17}O-excess LMDZ (per meg)	Reference
Vostok	−78.45	106.85	−14	−1	−20	−8	−1.4	−7	Vimeux et al. (2001a); Landais et al. (2008)
Dome C	−75.4	123.14	−6.5	−2.5	−13	−5.4	−2.6	−35	Stenni et al. (2004), unpublished
Taylos Dome	−77.28	158.26	−6.7	−6.6	2	−3.5	−4.6	−48	Stenni et al. (2004); Winkler et al. (2012)
Law Dome	−66.77	112.8	−7	–	4	−3.8	−1.3	−6.7	unpublished
EDML	−75.0	0.07	−6	−2.5	−2	−4.2	−2.6	−7.3	Stenni et al. (2004); Winkler et al. (2012)

Table 4. Slopes of d-excess and ^{17}O-excess as a function of RH_s. For the data, the slopes correspond to the regression lines shown in red in Fig. 1e, f. For LMDZ and the Merlivat and Jouzel (1979) closure equation, the "total" slope corresponds to the regression lines shown in blue and green in Fig. 1e, f. The "RH_s effect" is calculated by the difference between the "total" slope and the slope that we would obtain if RH_s was set to 60 % everywhere (RH_scste simulation for LMDZ). The "SST effect" is calculated by the difference between the slope that we would obtain if RH_s was set to 60 % everywhere, and the slope that we would obtain if RH_s was set to 60 % everywhere and if SST was set to 15 °C everywhere (RH_sSSTcste simulation for LMDZ).

Data/model	Total/RH_s effect/SST effect	d-excess vs. RH_s	^{17}O-excess vs. RH_s
data	total	−0.60	−0.60
closure equation	total	−0.58	−0.91
	RH_s effect	−0.16	−0.04
	SST effect	−0.43	−0.87
LMDZ	total	−0.22	−0.17
	RH_s effect	−0.15	−0.07
	SST effect	−0.06	0.01

^{17}O-excess (Fig. 1, dashed green). This can be visualized by plots of d-excess and ^{17}O-excess as a function of RH_s (Fig. 1e, f). Corresponding slopes are shown in Table 4. According to the Merlivat and Jouzel (1979) closure, 73 % of the d-excess decrease as a function of RH_s is due to the direct effect of RH_s, and the remaining is due to the effect of SST. Virtually all of the ^{17}O-excess decrease as a function of RH_s is due to the direct effect of RH_s. This is because SST has a very small effect on ^{17}O-excess due to its log definition (Landais et al., 2008). We notice that the Merlivat and Jouzel (1979) closure predicts a larger ^{17}O-excess-vs-RH_s slope than observed. This suggests that in nature some processes, such as boundary layer mixing with the free troposphere, act to dampen the ^{17}O-excess sensitivity to evaporative conditions.

The water vapor composition at the lowest model level simulated by LMDZ is compared to the data for each measurement day and location. LMDZ captures the RH_s distribution as a function of latitude well, with an increase in RH_s with latitude (Fig. 1a, blue). It also simulates the poleward decrease in δ^{18}O, d-excess and ^{17}O-excess. However, it overestimates the poleward decrease in δ^{18}O (by about 60 % from 35° S to 67° S) and underestimates the poleward decrease in d-excess (by about 65 %) and ^{17}O-excess (by about 70 %). As a result, the slopes of the RH_s-d-excess and RH_s-^{17}O-excess relationships are underestimated, by about 65 and 70 %, respectively (Fig. 1e, f, Table 4). The lack of sensitivity of d-excess to RH_s in LMDZ was already noticed when comparing to water vapor measurements in Greenland (Steen-Larsen et al., 2013).

This lack of sensitivity could be due to several kinds of problems. First, there could be problems in the composition of the evaporation flux. However, this does not appear to be the case, since the Merlivat and Jouzel (1979) closure approximation, which applies the same Craig and Gordon (1965) equation as in LMDZ, is in good agreement with the observations (Fig. 1e, f). Using the RH_sSSTcste and RH_scste simulations, we estimate that LMDZ underestimates the RH_s and SST effects in similar proportions: 37 and 31 %, respectively (Table 4). This suggests that in LMDZ, the sensitivity to SST and to RH_s are dampened by some atmospheric processes that are unrelated to evaporative conditions.

Second, there could be some altitude mismatch between the near-surface vapor collected on the ship (a few meters), and the vapor of the first layer of the model (0–130 m). This hypothesis is supported by the fact that the simulated δ^{18}O latitudinal gradient in the low-level vapor is steeper than in that observed in the near-surface vapor (Fig. 1a). As a simple interpolation, we calculate near-surface vapor δ^{18}O as

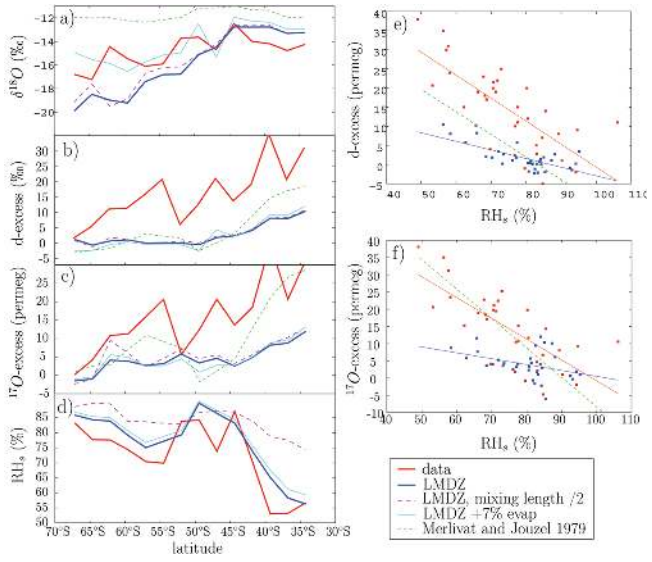

Fig. 1. δ^{18}O **(a)**, d-excess **(b)**, ^{17}O-excess **(c)** and RH$_s$ **(d)** of surface water vapor measured by Uemura et al. (2008, 2010) (red) and simulated by LMDZ (blue), as a function of latitude. Results are regridded on the LMDZ grid and applied a smoothing Gaussian filter of 10° in latitude. D-excess **(e)** and ^{17}O-excess **(f)** of surface water vapor measured by Uemura et al. (2008, 2010) and simulated by LMDZ, as a function of surface relative humidity RH$_s$. Model outputs were collocated with the measurements. Regression coefficients for both simulated and observed values are indicated in Table 4. For comparison, the d-excess and ^{17}O-excess of surface water vapor predicted by the Merlivat and Jouzel (1979) closure approximation (Appendix A) is also shown in green. For clarity, we show only the regression line. Sensitivity tests using the LMDZ model (purple and cyan) are detailed in the text

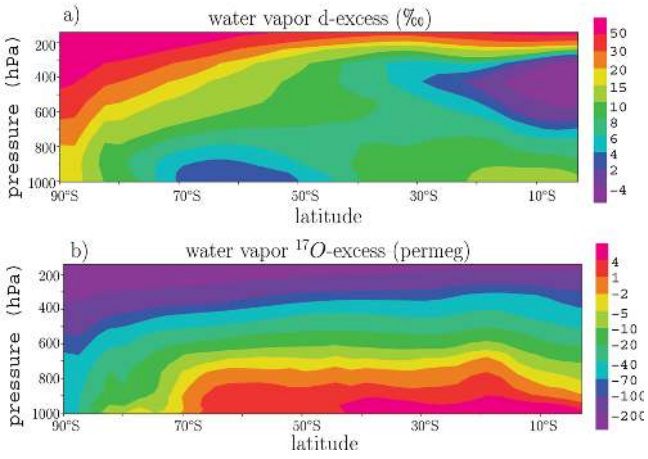

Fig. 2. Zonal mean of simulated d-excess **(a)** and ^{17}O-excess **(b)** in water vapor as a function of latitude and altitude in the Southern Hemisphere.

a mixture between the low-level vapor and the evaporation flux. When doing so, the δ^{18}O latitudinal gradient becomes less steep (Fig. 1a, cyan). Quantitatively, adding 7 % of surface evaporation appears optimal to match the observed variations in near-surface δ^{18}O. However, adding 7 % of evaporation flux has little influence on d-excess and ^{17}O-excess (Fig. 1b, c, cyan). Therefore, the altitude mismatch is unlikely to explain the d-excess and ^{17}O-excess mismatch.

Third, there could be problems in the boundary layer parameterization. If the boundary layer mixing is too strong, then the evaporative signal in the near-surface vapor may be dampened by advection of free-tropospheric air. Simulated latitudinal gradients of d-excess and of ^{17}O-excess in the free troposphere are smoother (or even reverted in the case of mid- and upper tropospheric d-excess) than near the surface (Fig. 2). A weaker vertical mixing might thus improve the results. To test this hypothesis, the mixing length scale used in the boundary layer parameterization is halved (Fig. 1 purple). However, this does little to improve d-excess or ^{17}O-excess.

Fourth, there could be all kinds of other problems affecting the latitudinal gradients in the free-tropospheric vapor, which is entrained into the boundary layer. In particular, some processes in the subtropics that lower the tropospheric d-excess and ^{17}O-excess could be oversimulated in the model (e.g. liquid condensation for d-excess, mixing for ^{17}O-excess), and other processes that increase the tropospheric d-excess and ^{17}O-excess could be undersimulated (e.g. rain drop re-evaporation). The range of processes that could be misrepresented is very large and the sensitivity tests that we have done so far have not allowed us to identify the culprit yet. Measurements of horizontal and vertical gradients in water vapor composition during cruises and aircraft campaigns would be useful to elucidate this problem. In the meanwhile, when interpreting the results in Sect. 4, we need to remember that the effect of evaporative conditions will be likely underestimated.

3.2 Spatial distribution

The simulated spatial patterns of annual mean δ^{18}O, d-excess and ^{17}O-excess in precipitation are compared with observations in Fig. 3. The latitudinal gradients are summarized in Fig. 4. In the latter figure, model outputs and observations are collocated for a more quantitative comparison.

The simulated annual mean spatial and zonal distribution of δ^{18}O and d-excess were already extensively evaluated in Risi et al. (2010b). Spatial patterns of δ^{18}O are very well captured, including the main "effects" that have long been documented (Dansgaard, 1964; Rozanski et al., 1993): latitudinal gradient associated with the temperature effect, the land-sea contrast with more depleted values over land associated with the continental effect, and the depletion of the South Asia–Western Pacific region, associated with the amount effect. The root mean square error of simulated δ^{18}O is 3.5 ‰ globally. The latitudinal gradient in polar regions is underestimated, due to the warm bias in these regions (Risi et al., 2010b).

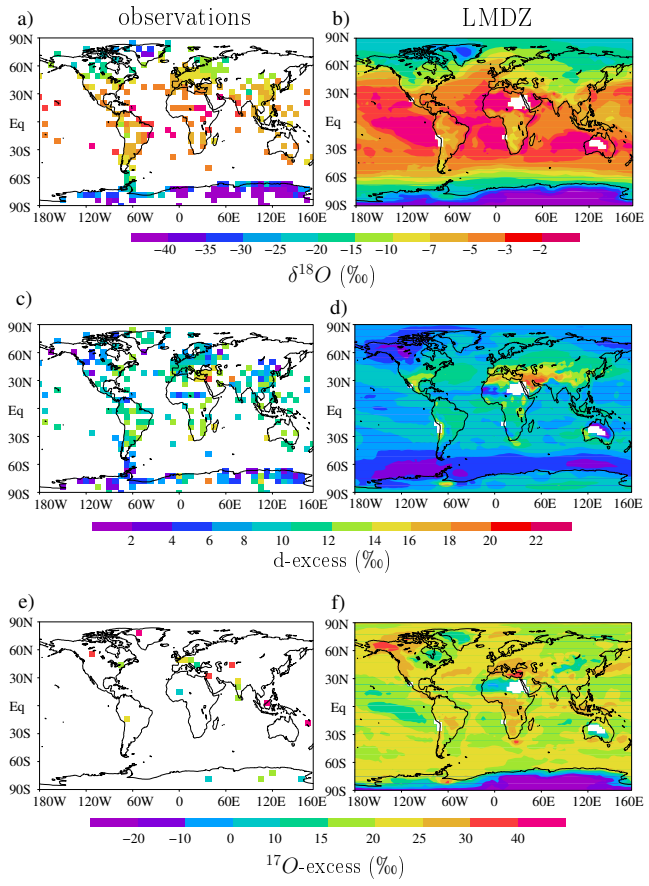

Fig. 3. Annual mean of precipitation $\delta^{18}O$, d-excess and ^{17}O-excess simulated by LMDZ and observed by the GNIP network and various observations listed in Tables 1 and 2.

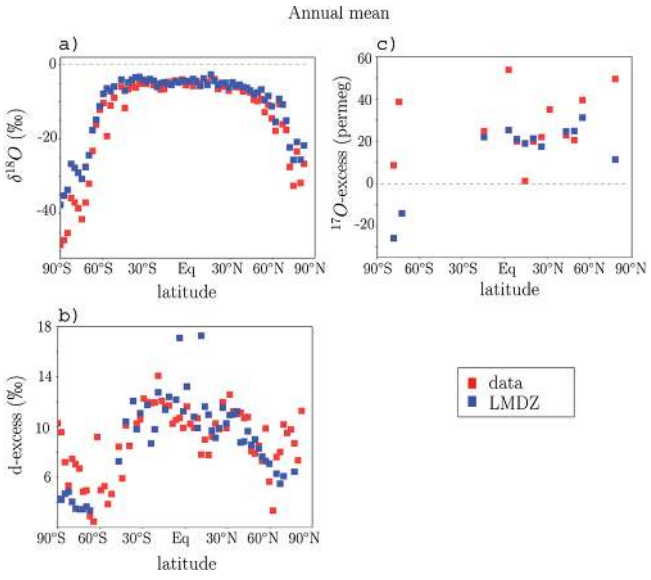

Fig. 4. Annual, zonal mean of precipitation $\delta^{18}O$, d-excess and ^{17}O-excess simulated by LMDZ, compared to the GNIP database for $\delta^{18}O$ and d-excess and to the data listed in Tables 1 and 2 for ^{17}O-excess. The model outputs are collocated with the location and month of each measurement.

Spatial patterns for d-excess are also relatively well captured: a minimum in the Southern Ocean and over the coasts of Antarctica, a minimum over northwestern America and Alaska, a minimum over the Sahel region (associated with rain re-evaporation; Risi et al., 2008b) and a maximum over the Mediterranean and Middle East region (interpreted as the effect of strong kinetic fractionation during sea surface evaporation in a dry environment, Gat et al., 1996). Even the land-sea contrast with higher values over land, traditionally interpreted as the effect of fractionation during continental recycling (Gat and Matsui, 1991), is well captured by the model even without representing this process. The latitudinal structure, with a local minimum near the equator, maxima in the subtropics, a strong poleward decrease in mid-latitudes, and a poleward increase in high latitudes ($> 60°$), are well captured (Fig. 4). The root mean square error is only 3.2 ‰ globally.

It is surprising that LMDZ simulates the latitudinal gradient of precipitation d-excess well, while it had difficulties simulating it in the vapor. In particular in the subtropics, precipitation d-excess has the right mean value in spite of the vapor d-excess being underestimated by about 20 ‰ (Sect. 3.1). It could be that d-excess in precipitation reflects the d-excess in the vapor at a level where LMDZ would agree better with observations, if such observations existed. It could also be that the correct values of precipitation d-excess arises from a compensation of errors. In particular, the parameter ϕ controlling kinetic fractionation during rain re-evaporation was tuned to optimize precipitation d-excess (Risi et al., 2010b). Simultaneous measurements of d-excess in both vapor and precipitation would be very helpful to ensure that tuning ϕ does not lead to error compensations.

No coherent spatial pattern for ^{17}O-excess emerges from the sparse data available. Measured values range from about 0 to 50 per meg. The values simulated by LMDZ are within this range, except in Antarctica and Greenland where values are underestimated by about 40 per meg. Outside these two regions, the root mean square error is 13 per meg. The underestimate of ^{17}O-excess in subtropical water vapor source (Sect. 3.1) could contribute to the underestimate of polar ^{17}O-excess. As will be detailed in Sect. 4.4, uncertainties in supersaturation parameter λ and in the equilibrium fractionation and diffusivity coefficients may also contribute to LMDZ difficulties in simulating polar ^{17}O-excess.

3.3 Seasonal variations

The simulated latitudinal pattern of seasonal variations (JJA-DJF) in δ^{18}O, d-excess and ^{17}O-excess are compared with observations in Fig. 5. The seasonality in δ^{18}O is very well captured by the model, with a root mean square error of

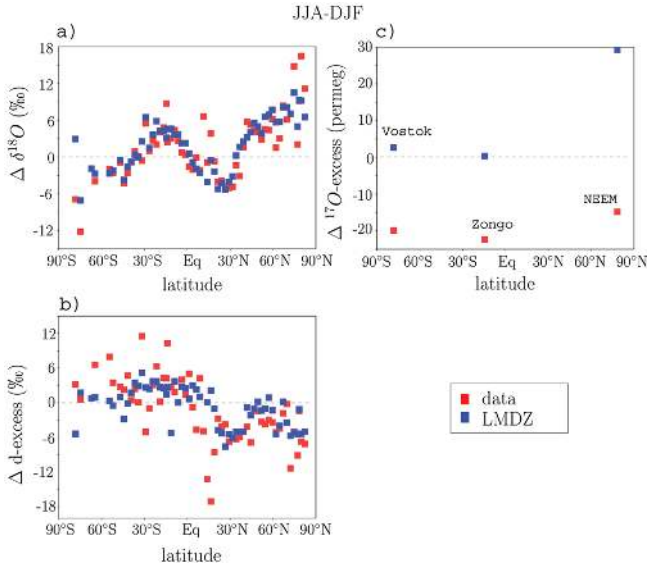

Fig. 5. Same as Fig. 4 but for JJA-DJF variations.

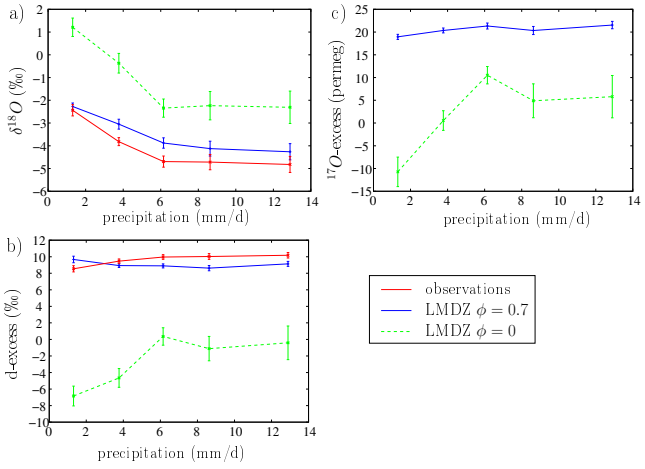

Fig. 6. Composites of precipitation δ^{18}O, d-excess and ^{17}O-excess as a function of precipitation, in the control simulation of LMDZ, in a test in which $\phi = 0$, and in observations. Precipitation range was divided into five bins for the composites. Error bars represent the standard deviation within each bin divided by the square root of the number of samples in the bin. LMDZ outputs were collocated with the GNIP observations they are compared with. All GNIP observations in oceanic or coastal stations (altitude lower than 20 m) in the tropics (equatorward of 30°) are used. No ^{17}O-excess data are shown due to the lack of data.

2.7 ‰. In the tropics, precipitation is more depleted during the wet season, consistent with the amount effect. Poleward of 35° latitude, precipitation is more depleted in winter, consistent with the temperature effect (Dansgaard, 1964).

The broad pattern of d-excess seasonality is well captured. In most regions of the globe, observed d-excess is lower in summer of each hemisphere, especially in the subtropics. This is also the case in LMDZ, but with less noise. The root mean square error is 4.8 ‰. The d-excess seasonality in high latitudes has often been interpreted as the effect of evaporative conditions at the moisture source (e.g. Delmotte et al., 2000). It is surprising that although LMDZ underestimates the d-excess sensitivity to evaporative conditions (Sect. 3.1), LMDZ is able to capture the observed d-excess seasonality in northern high latitudes. This may be because d-excess seasonality in these regions arises at least partly from processes other than changes in evaporative conditions. LMDZ fails to simulate the higher d-excess in winter in Central Antarctica. As will be detailed in Sect. 4.4, this could be associated with uncertainties in the supersaturation parameter λ.

We have only three sites where seasonal cycles of ^{17}O-excess in precipitation are available: in Greenland, Antarctica and Bolivia. Observed ^{17}O-excess is 15 per meg lower in summer in Greenland, a few per meg higher in winter in Antarctica, and 22 per meg lower during the dry season in Bolivia. LMDZ fails at capturing the correct seasonality at all sites.

Simulated d-excess and ^{17}O-excess in tropical regions are very sensitive to the choice of the re-evaporation parameter ϕ. Figure 6 shows the sensitivity of δ^{18}O, d-excess and ^{17}O-excess to this parameter. When $\phi = 0$, the relative humidity around rain drops is that of the environment and kinetic fractionation is stronger. In this case, δ^{18}O increases and d-excess and ^{17}O-excess decrease especially in dry regions. Over the Bolivian site however, tuning ϕ is not sufficient to reach model-data agreement. In observations, ^{17}O-excess is 22 per meg lower during the dry season than during the wet season, possibly due to more rain re-evaporation during the dry season. However, even with $\phi = 0$ (maximum kinetic fractionation during re-evaporation), ^{17}O-excess is only 3 per meg lower during the dry season than during the wet season. Therefore, processes other than re-evaporation may be at play in this region, and LMDZ does not capture them. For example, the observed 4 ‰ higher d-excess during the dry season may be associated with a higher proportion of the moisture arising from bare soil evaporation upstream, which is characterized by higher d-excess (Gat and Matsui, 1991). LMDZ does not simulate this effect.

3.4 Last glacial maximum

LGM-PD variations for δ^{18}O and d-excess were extensively evaluated in Risi et al. (2010b). We focus here on LGM-PD variations in Antarctica where most of the LGM ^{17}O-excess data are available. LMDZ simulates qualitatively well the observed depletion at LGM in Antarctica, and it captures the increased depletion towards the interior (Fig. 7a). However, the depletion magnitude is underestimated by 20 % in Dome C and up to 45 % in Vostok and Taylor Dome (Table 3).

Although simulating d-excess signals with the same sign as δ^{18}O has proven difficult for some models (Werner et al.,

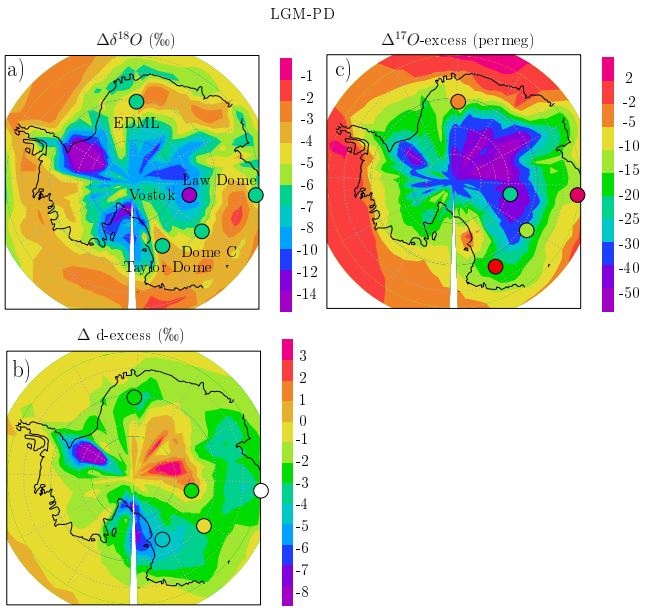

Fig. 7. LGM minus present-day difference in precipitation $\delta^{18}O$, d-excess and ^{17}O-excess in Antarctica observed in ice cores (colored circles) and simulated (shaded) by LMDZ over Antarctica. Numerical values are given in Table 3.

2001; Noone, 2008), LMDZ is able to simulate the lower d-excess at LGM over most of Antarctica (Fig. 7b). In observations, the decrease of d-excess from PD to LGM is all the larger as we go poleward. However, LMDZ simulates the opposite, with an increase over Central Antarctica from PD to LGM. When using the LGM SST forcing based on the IPSL climate simulation, the decrease of d-excess from LGM to PD is 1 ‰ stronger but has a similar shape (Risi et al., 2010b).

LMDZ captures the lower ^{17}O-excess observed at LGM at most sites (Fig. 7c). In observations, the decrease of ^{17}O-excess from PD to LGM is all the larger as we go poleward, as for d-excess. This is also well captured by LMDZ. However, LMDZ overestimates the ^{17}O-excess decrease from PD to LGM at all sites, and simulates the wrong sign near the coast. Note that stratospheric intrusions may contribute to the LGM-PD difference in ^{17}O-excess (Winkler et al., 2013), but their effects are neglected in LMDZ.

4 Understanding what controls precipitation ^{17}O-excess

We now use LMDZ simulations to understand what controls δ^{18}O, d-excess and ^{17}O-excess in the model. In doing so, we keep in mind the strengths and weaknesses highlighted by the model-data comparison: we have good confidence in the δ^{18}O distribution both for PD and LGM. We have relatively good confidence in the annual-mean d-excess distribution and in the broad latitudinal pattern of d-excess seasonality. Finally, we have moderate confidence in the LGM-PD changes in d-excess and ^{17}O-excess in Antarctica. All other features are subject to more caution, as they are either misrepresented in LMDZ, or difficult to evaluate given the lack of data.

Figure 8 shows the decomposition of the latitudinal variations of annual mean δ^{18}O, d-excess and ^{17}O-excess into four effects (Sect. 2.4): (1) precipitation-vapor difference (green); (2) evaporative conditions associated with SST and RH_s (orange); (3) effect of supersaturation (dashed pink); and (4) all other processes (red). The sum of all these contributions make the total signal (black). Figure 9 and 10 shows the same decomposition for seasonal and LGM-PD variations, respectively.

4.1 Precipitation-vapor difference

The contribution of precipitation-vapor difference to the precipitation signal is shown in green in Figs. 8–10.

4.1.1 Rain re-evaporation

In the tropics, in the absence of rain re-evaporation, the precipitation reequilibrates with the vapor as it falls (Risi et al., 2008a). Variations in precipitation-vapor difference are thus mainly associated with rain re-evaporation.

As rain re-evaporates, δ^{18}O increases in the rain (Risi et al., 2008a, 2010a; Lee and Fung, 2008). This process is the main reason for the so-called amount effect (Risi et al., 2008a), i.e. the decrease of δ^{18}O as precipitation amount increases. Regarding the latitudinal gradient, the green and black curves have similar shapes for δ^{18}O (Fig. 8a). This means that rain re-evaporation explains much of the latitudinal variations in precipitation δ^{18}O. In particular, rain re-evaporation explains the slight local minimum in δ^{18}O in the equatorial region (around 0° N) where the air is moist, and the larger values in the subtropics (around 30° N and 35° S) where re-evaporation is strong. Regarding seasonality, in the tropics, the green and black curves also have a similar shape for δ^{18}O (Fig. 9). This means that the effect of rain re-evaporation dominates the seasonality in δ^{18}O, with larger values during the dry season (Fig. 9a, Risi et al., 2008b). At LGM, LMDZ simulates only small changes in δ^{18}O in the tropics, but the latitudinal distribution of these changes mirror those in precipitation-vapor difference.

As rain re-evaporates, in parallel to the δ^{18}O increase, d-excess and ^{17}O-excess both decrease (Risi et al., 2010a; Barras and Simmonds, 2009; Landais et al., 2010). In the tropics, this explains much of the latitudinal variations, in particular the local maxima in d-excess and ^{17}O-excess in the equatorial region and the lower values in the subtropics (Fig. 8b, c). Rain re-evaporation also dominates the seasonality in ^{17}O-excess (and to a lesser extent in d-excess), with lower values during the dry season (Fig. 9b, c). This seasonal evolution

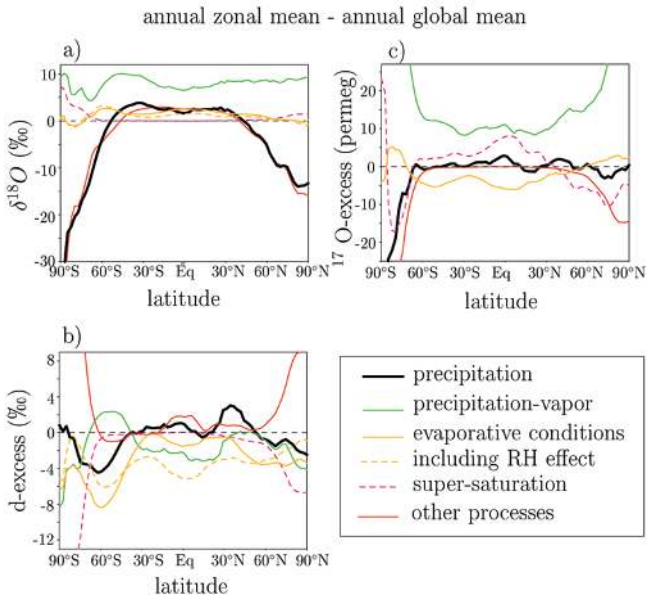

Fig. 8. Decomposition of the annual zonal mean distribution of the precipitation δ^{18}O, d-excess and ^{17}O-excess into different contributions. The black line correspond to the total simulated values. The green, orange, dashed pink and red correspond to the precipitation-vapor difference, the effect of evaporative conditions (SST and RH_s), the effect of supersaturation and all other effects, respectively. Their sum makes the total black line. The effect of evaporative conditions is further decomposed into the effect of RH_s only (dashed orange). The difference between the solid and dashed orange lines correspond to the effect of SST only. To focus on spatial patterns, we subtract the annual, global mean to all curves. When the black curve is positive, δ^{18}O, d-excess or ^{17}O-excess are higher than the global mean. When the colored curves are positive, the corresponding process contributes to increase the total values. When the colored curves show a similar shape as the black curve, they contribute to the latitudinal variations of the total signal.

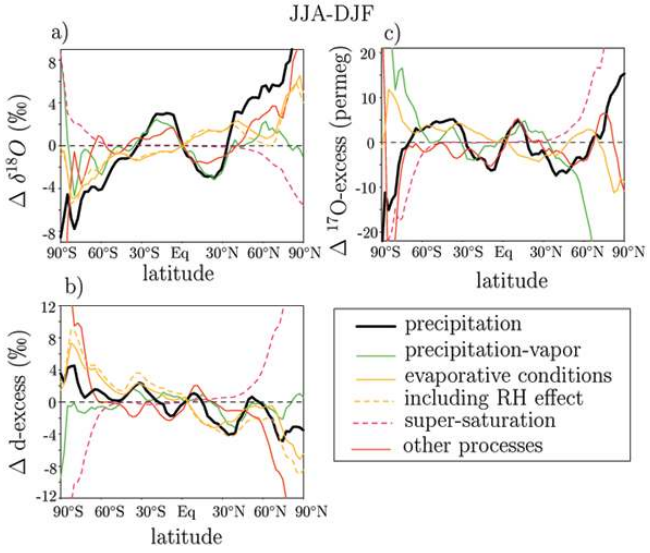

Fig. 9. Same as figure 8, but for JJA-DJF differences. When the black line is positive, the $\delta^{18}O$, d-excess or ^{17}O -excess values are higher in JJA than in DJF (i.e. higher in summer in the northern Hemisphere, higher in winter in the Southern Hemisphere, higher during the wet season in the northern tropics, higher during the dry season in the southern tropics). When the colored curves are of the same sign as the black curves, then the corresponding process contributes positively to the total seasonal signal.

of the triple isotopic composition of precipitation is consistent with that observed during the transition from dry to wet season in the Sahel (Risi et al., 2008b; Landais et al., 2010). At LGM also, the small changes in d-excess and ^{17}O-excess in the tropics reflect the changes in rain re-evaporation (Fig. 10b, c).

4.1.2 Effect of fractionation coefficients

In high latitudes, precipitation falls as snow and is thus not affected as much by post-condensational processes. The precipitation-vapor difference is thus associated with condensation processes. As temperature decreases, the fractionation coefficients increase, but the coefficient for δ^{18}O increases faster than that for δD. Therefore, precipitation-vapor difference for d-excess becomes more negative at colder temperatures. This contributes to the lower d-excess in polar regions, during winter and during the LGM (Figs. 8b, 9b and 10b). During winter, this effect is not major and does not prevent d-excess to be higher in winter. During the LGM in contrast, this effect appears as the main process contributing to the lower d-excess in polar regions.

Similarly, the precipitation-vapor difference in ^{17}O-excess increases at lower temperatures. This is due to the fact that the slope of the meteorologic water line (0.528) is lower than the logarithm of the ratio of the fractionation coefficients ($\frac{\ln(\alpha_{O17})}{\ln(\alpha_{O18})} = 0.529$). This fractionation coefficient effect contributes to the increase of ^{17}O-excess in polar regions, in winter and at LGM. This effect might however be overestimated in LMDZ. Observations at the NEEM station in Greenland shows that ^{17}O-excess is only 3 ± 13 per meg higher in the snow than in the vapor (Landais et al., 2012b), compared to 41 per meg higher as predicted by LMDZ (not shown). This may be due to $\frac{\ln(\alpha_{O17})}{\ln(\alpha_{O18})}$ being actually closer to 0.528 than to 0.529 for vapor-solid equilibrium (Landais et al., 2012b). However, even in LMDZ, this equilibrium fractionation effect is not dominant since it is overwhelmed by other effects (green and black curves do not have similar shapes and often have opposite signs on Figs. 8c, 9c and 10c).

4.2 Evaporative conditions

The contribution of evaporative conditions (SST and RH_s) to the precipitation signal is shown in orange in Figs. 8–10. The role of RH_s only is shown in dashed orange. The difference

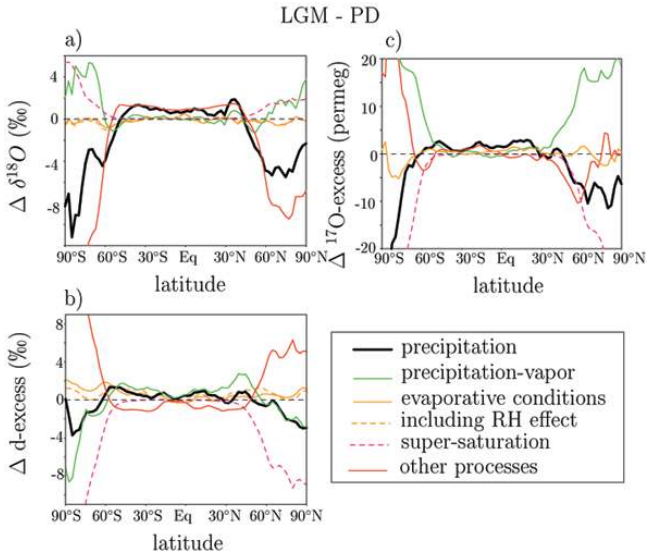

Fig. 10. Same as Fig. 8, but for LGM-PD difference. When the black line is positive, the $\delta^{18}O$, d-excess or ^{17}O -excess values are higher in LGM than in PD. When the colored curves are of the same sign as the black curves, then the corresponding process contributes positively to the total LGM-PD signal.

between the solid and dashed lines correspond to the role of SST only.

For δ^{18}O, evaporative conditions play little role in the latitudinal gradient and in LGM-PD differences, but they do contribute to the seasonality of δ^{18}O in high latitudes. This is mainly due to the RH_s being drier in summer.

Evaporative conditions play a more important role for the distribution of d-excess. In particular, the poleward decrease in d-excess from 30° to 60° in the Southern Ocean is due to evaporative conditions (Fig. 8b). SST and RH_s account each for about half of this decrease. The broad latitudinal distribution of d-excess seasonality was characterized both in observations and LMDZ by lower values in summer in the subtropics and mid-latitudes of each hemisphere (Sect. 3, Fig. 5). This pattern is similar to that of the evaporative condition contribution, in particular the effect of RH_s at the moisture source (Fig. 9b). Therefore, the observed d-excess pattern could be due to the RH_s seasonality at the moisture source or to seasonal shifts in moisture sources. In high latitudes, the contributions of "other processes" (red curve, detailed in Sect.4.3) and of supersaturation (pink curve) effects are large and largely compensate each other (later discussion in Sect. 4.3). Beside these two components, the dominant cause for d-excess seasonality in polar regions is RH_s conditions at the moisture source (Fig. 9b). The importance of evaporative conditions could be even stronger in nature than in LMDZ, since LMDZ underestimates the effect of RH_s and SST on d-excess.

Regarding LGM-PD differences, in LMDZ changes in evaporative conditions play little role in decreasing d-excess at LGM. This is because RH_s and SST do not vary as much between LGM and present as during a seasonal cycle. This contradicts the suggestion that higher RH_s at the LGM (Jouzel et al., 1982) or lower SST at the moisture source (Stenni et al., 2001) contribute to the lower d-excess in Antarctica. It is possible that the contribution of evaporative conditions was significant at LGM, that it is underestimated by LMDZ, and that LMDZ gets the right sign of d-excess change through compensation of errors. This study just shows that the lower d-excess at LGM can be explained without change in evaporative conditions, provided that a significant supersaturation parameter is chosen.

For ^{17}O-excess, the solid and dashed orange lines are identical, since SST has no impact on ^{17}O-excess at evaporation (Risi et al., 2010c). LMDZ simulates a small role for evaporative conditions in the latitudinal gradient of ^{17}O-excess (Fig. 8c). However, we have shown in Sect. 3.1 that LMDZ underestimates the slope of ^{17}O-excess as a function of RH_s. Therefore, in nature the role for evaporative conditions might be stronger. For LGM-PD differences, the evaporative condition effect is not negligible in Antarctica. The effect of RH_s at the moisture source leads to lower ^{17}O-excess by 5 per meg at Vostok. If LMDZ had a more realistic RH_s-^{17}O-excess slope (i.e. about 4 times larger), the RH_s contribution might have been larger, in better agreement with Landais et al. (2008). LMDZ can however simulate the observed lower ^{17}O-excess at LGM without an important role of evaporative conditions, provided that an adequate supersaturation parameter is used (Sect. 4.4).

4.3 Convective processes, distillation and mixing between vapors of different origins

The sum of all effects other than supersaturation, precip-vapor difference and evaporative conditions is shown in red.

4.3.1 Convective processes

In the tropics, the air temperature is relatively uniform horizontally (Sobel and Bretherton, 2000) so the temperature effect is small (Rozanski et al., 1993). Large variations in humidity can however be associated with vertical motions (Sherwood, 1996). Since δ^{18}O decreases with altitude (e.g. Ehhalt, 1974), subsidence of air in unsaturated downdrafts of convective systems (Risi et al., 2008a) and the subsidence at the large scale in dry regions (Frankenberg et al., 2009; Galewsky and Hurley, 2010) both deplete the water vapor. In addition, rain re-evaporation and rain–vapor interactions in moist conditions can also deplete the vapor (Lawrence et al., 2004; Worden et al., 2007). Therefore, in the tropics, the red curves in Figs. 8–10 correspond to the combined effects of large-scale dynamics, of unsaturated downdrafts and of rain re-evaporation on the vapor. We can see that these effects are the major contribution to explain the seasonality in δ^{18}O in the tropics (Fig. 9). This is consistent with the important role

of unsaturated downdrafts in the amount effect (Risi et al., 2008a).

For d-excess, the vertical gradient in the tropics remains an open question. LMDZ simulates a decrease with altitude (Fig. 2a), whereas theoretical considerations (Bony et al., 2008) and indirect evidence based on upper-tropospheric measurements (Sayres et al., 2010) and high-frequency measurements (Lai and Ehleringer, 2011; Welp et al., 2012; Wen et al., 2010) suggest that d-excess increases with altitude. Therefore, the role of convective-scale subsidence on d-excess is unclear. In contrast, it is more certain that rain re-evaporation and rain–vapor interactions increase the d-excess of the vapor (Landais et al., 2010). This process explains the maximum of d-excess in equatorial convective regions (Fig. 8b). This is also a major contribution to the seasonality in d-excess in the tropics (Fig. 9b).

For ^{17}O-excess, the vertical gradient in the tropics also remains an open question. As for d-excess, rain re-evaporation and rain–vapor interactions increase the ^{17}O-excess of the vapor (Landais et al., 2010). This process is the major contribution to explain the seasonality in ^{17}O-excess in the tropics (Fig. 9c).

4.3.2 Distillation and mixing

In high latitudes, the above-mentioned processes play a minor role. Therefore, the red curves represent the combined effects of distillation and mixing between vapor of different origins (hereafter shortened as "mixing"). In particular, mixing includes evaporative recycling along trajectories, i.e. mixing between vapor undergoing distillation during its poleward transport and newly evaporated vapor from the ocean surface.

Distillation decreases δ^{18}O. Simple Rayleigh distillation calculations based on LMDZ temperature show that if there was only distillation, the δ^{18}O latitudinal gradient would be four times larger than actually simulated (not shown). In reality and in the simulations, this latitudinal gradient is dampened by evaporative recycling along trajectories. As expected, distillation and mixing (red curve) dominate the δ^{18}O latitudinal gradient, consistent with the traditional temperature effect (Dansgaard, 1964). It also dominates the seasonality and the LGM-PD difference in δ^{18}O.

For d-excess, Rayleigh distillation increases d-excess at low temperature (Jouzel and Merlivat, 1984). This explains the polar increase of the red contribution (Fig. 8b). For the same reasons, in high latitudes, the Rayleigh effect contributes to the increased d-excess in winter (Fig. 9b) and at LGM (Fig. 10b).

For ^{17}O-excess, the poleward decrease of the red contribution in high latitudes (Fig. 8c) may be due to the effect of evaporative recycling. The effect of evaporative recycling on ^{17}O-excess is due to the fact that mixing of two air masses with very different δ^{18}O leads to ^{17}O-excess values that are lower than both end-members (Risi et al., 2010c). The fact that LMDZ underestimates ^{17}O-excess in polar regions (Sect. 3.2) may be due to the fact that the advection scheme is too diffusive. Indeed, in the Van Leer (1977) advection scheme, advection of vapor from one grid box A to neighboring grid box B is represented as mixing between of vapor A and B into grid box B.

Note that there is persistent uncertainty on vapor-solid fractionation used for distillation at very low temperature. Vapor-solid fractionation coefficients have been measured only down to $-34\,^{\circ}$C and are extrapolated beyond (Majoube, 1971a), leading to some uncertainty. There are also disagreements between different experimental measurements (Ellehoej, 2011). This may contribute to difficulties simulating d-excess and ^{17}O-excess in polar regions.

4.4 Supersaturation

The effect of supersaturation is shown in dashed pink in Figs. 8–10.

Supersaturation occurs at cold temperatures, in polar regions, and this partially compensates the effect of distillation. When supersaturation occurs, δ^{18}O decreases less along trajectories than expected. The supersaturation effect has, however, relatively little effect on δ^{18}O (Fig. 8a; pink).

For d-excess and ^{17}O-excess, supersaturation has a larger effect. The distillation/mixing and supersaturation effects are both very large and largely compensate each other (Fig. 8b,c). When supersaturation occurs, d-excess and ^{17}O-excess increase less along trajectories than expected. As a consequence, the sign of the seasonality and of LGM-PD variations results from a balance between distillation effects and supersaturation effects. Regarding seasonality for example, in Greenland where LMDZ captures the sign of the d-excess seasonality, the distillation effect dominates and this leads to higher d-excess values in winter when the distillation is stronger. In Vostok in contrast, d-excess is higher in winter in observations but lower in winter in LMDZ. This suggests that in observations, the distillation effect dominates, but that in LMDZ, the supersaturation effect is too strong and dominates. In observations, ^{17}O-excess is higher in winter in Greenland and lower in winter in Antarctica. This suggests that the supersaturation effect dominates in Antarctica but not in Greenland. In LMDZ, the seasonality is misrepresented in both regions.

Summing up large effects of different signs without having good confidence in their magnitude leads to strong uncertainty. Estimating their magnitude calls for laboratory experiments. In particular, d-excess and ^{17}O-excess in polar regions is extremely sensitive to the choice of λ, consistent with simple model studies (Ciais and Jouzel, 1994; Winkler et al., 2012; Landais et al., 2012a,b). Risi et al. (2010b) chose λ to optimize the latitudinal gradient in polar d-excess. If λ was lower, the agreement would be better for ^{17}O-excess, but d-excess would be overestimated in Central Antarctica (Fig. 11b,c). In LMDZ, we cannot tune λ to agree both with

Table 5. Summary of the main processes explaining the main features of the $\delta^{18}O$, d-excess and ^{17}O-excess spatio-temporal distribution in the LMDZ model, as a function of latitude. The physical meaning of these processes are detailed in Sect. 4. Mixing refers to mixing of water vapor of different origins.

Isotopic tracer		δ^{18}O	d-excess	^{17}O-excess
Tropics	latitudinal gradient	re-evaporation	re-evaporation	re-evaporation
	seasonal variation	re-evaporation + convection	re-evaporation + convection	convection + re-evaporation
	LGM – PD difference	ocean composition	re-evaporation	re-evaporation
Mid-latitudes	latitudinal gradient	distillation	SST + RH_s	distillation/mixing
	seasonal variation	distillation	RH_s + condensation conditions	distillation/mixing
	LGM – PD difference	distillation	condensation conditions	distillation/mixing
High latitudes	latitudinal gradient	distillation	distillation + supersaturation	distillation/mixing + supersaturation
	seasonal variation	distillation + RH_s	RH_s + distillation + supersaturation	distillation/mixing + supersaturation
	LGM – PD difference	distillation	distillation + supersaturation	distillation/mixing + supersaturation

d-excess and ^{17}O-excess. The sensitivity to a poorly constrained parameter makes the interpretation of d-excess and ^{17}O-excess LGM-PD changes difficult. Any observed change at a given location can be reproduced by any model by tuning λ. Setting $\lambda = 0.004$ leads to a good agreement with the LGM-PD variations, but a lower value of λ can lead to a reversal of the sign of the d-excess and ^{17}O excess LGM-PD variations (Fig. 11e,f).

In addition, there are uncertainties on the diffusivity coefficients. Cappa et al. (2003) and Merlivat and Jouzel (1979) found different values and Luz et al. (2009) suggest that they may actually vary also with temperature. Therefore, the combined uncertainties on supersaturation, equilibrium fractionation, and diffusivity coefficients make it difficult to interpret d-excess and ^{17}O-excess data and to identify the culprit in the shortcomings of the d-excess and ^{17}O-excess simulation in polar regions. In addition, stratospheric intrusions cannot be ruled out to explain at least part of the measured signals in ^{17}O-excess (Winkler et al., 2013).

5 Conclusion and perspectives

We used the LMDZ GCM to simulate the PD and LGM distributions of precipitation δ^{18}O, d-excess and ^{17}O-excess. LMDZ correctly captures the δ^{18}O distribution and climatic variations. After appropriate tuning of supersaturation, it captures reasonably well the d-excess distribution and the average LGM-PD variations in Antarctica. For ^{17}O-excess, the lack of data makes it difficult to evaluate the spatio-temporal distribution. LMDZ underestimates the ^{17}O-excess latitudinal gradient in the Austral Ocean water vapor and has difficulties to simulate seasonal variations on some stations.

We propose a methodology to quantify the controlling factors of the associated latitudinal, seasonal and LGM-PD variations. Table 5 summarizes the main factors controlling the different aspects of the δ^{18}O, d-excess and ^{17}O-excess spatio-temporal distribution depending on latitude. In the tropics, rain re-evaporation and convective processes explain the main features of the δ^{18}O, d-excess and ^{17}O-excess spatio-temporal distributions. In mid- and high-latitude, as expected, the distillation effect is the first-order control on δ^{18}O. D-excess and ^{17}O-excess are affected by distillation, but also by other processes. Evaporative conditions play a role for d-excess, and may also play a role for ^{17}O-excess if LMDZ was more sensitive to RH_s and SST. The sensitivity to evaporative conditions is an added value of d-excess compared to δ^{18}O, consistent with previous studies (e.g. Vimeux et al., 1999, 2001b; Gat, 2000; Stenni et al., 2001; Masson-Delmotte et al., 2005). ^{17}O-excess also features this added value, but an additional particularity is its sensitivity to mixing between vapor of different origins along distillation trajectories. ^{17}O-excess seems to be sensitive to a much broader

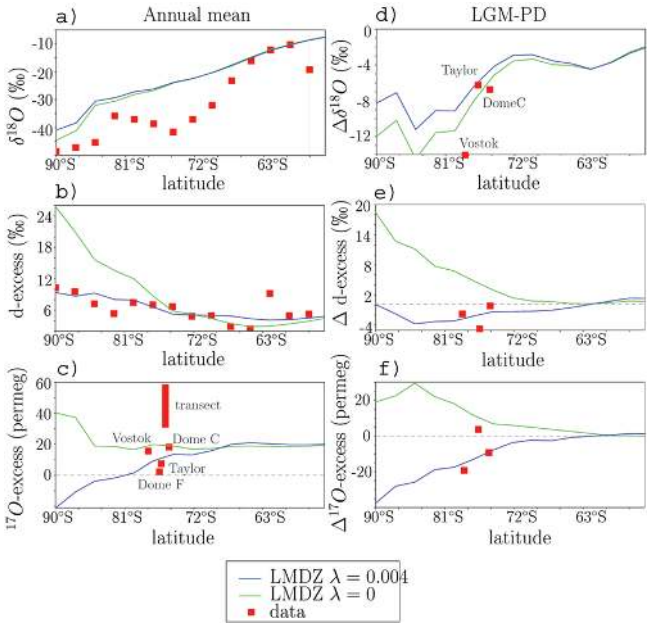

Fig. 11. (a–c) Zonal, annual mean δ^{18}O, d-excess and ^{17}O-excess in precipitation in Antarctica simulated by LMDZ for the control value of λ (blue) and when λ is set to 0 (green). Model outputs are collocated with observations. **(d–f)** Same for zonal, annual mean LGM-PD difference. In all plots, model outputs are compared qualitatively (i.e. with no collocation) with observations (black squares). For δ^{18}O and d-excess, values are zonal averages from the GNIP-Antarctica data set regridded on LMDZ grid. For ^{17}O-excess, numerical values are those given in Tables 2 and 3.

range of processes. Determining the controlling factors in nature with more confidence would however require much more data to more comprehensively evaluate GCM simulations of ^{17}O-excess. Continuous, in situ water vapor measurements are needed in order to improve the understanding of the driving mechanisms of d-excess and ^{17}O-excess. In this regard the new laser-based techniques are extremely helpful for in situ isotope measurements of water vapor. Yet, it is not possible, at least so far, to determine ^{17}O-excess with the required precision (≤ 5 per meg) using this technology. Such measurements would be very helpful.

Supersaturation effects play a major role on both d-excess and ^{17}O-excess, leading to a large uncertainty in their interpretation. At LGM in polar regions, distillation and mixing effects tend to increase d-excess and ^{17}O-excess values, while supersaturation effects tend to decrease them. The balance between these two large effects is very sensitive to the assumed supersaturation function. Using a supersaturation function that leads to d-excess and ^{17}O-excess consistent with PD observations, LMDZ is able to simulate the lower d-excess and ^{17}O-excess at LGM without requiring any effect of changes in evaporative conditions at the moisture source. The choice of the supersaturation function, together with uncertainties in equilibrium fractionation and diffusivity coefficients, remain a key uncertainty in interpreting d-excess and ^{17}O-excess, since its choice determines the sign of LGM-PD changes. Measurements of vapor and precipitation along Antarctica transects would be very helpful to better constrain this function. New laboratory experiments focused on fractionation during ice formation in cold conditions would also be helpful.

We acknowledge the limitations inherent to our GCM simulations. The sensitivity of d-excess and ^{17}O-excess to ocean evaporative conditions is underestimated, for reasons that we do not understand but that are more likely related to free-tropospheric processes. Vertical profiles or latitudinal gradients of ^{17}O-excess in the free-tropospheric vapor would be helpful to diagnose the cause of these problems. Alternatively, comparison with other isotopic GCMs that do not feature the same bias, if these exist, could provide some insight. Finally, taking into account fractionation during bare soil evaporation (e.g. Gat and Matsui, 1991) may be necessary to interpret d-excess and ^{17}O-excess patterns over land.

Finally, the methodology presented here to decompose the isotopic signals into the different physical processes will remain valid for all GCMs. Applying this methodology to other GCMs will help extract robust features among models. If in the future, some GCMs are able to better simulate d-excess and ^{17}O-excess, applying this methodology to these GCMs will help understand what controls d-excess and ^{17}O-excess with more confidence.

Appendix A

Predicting the isotopic composition of the boundary layer vapor using the closure assumption

The simplest equation to predict the isotopic composition of the boundary layer vapor is the Merlivat and Jouzel (1979) closure. Although it fails to predict the absolute values of δ^{18}O and d-excess (Jouzel and Koster, 1996), it has been shown to accurately predict the sensitivity of the isotopic composition to ocean surface conditions (Uemura et al., 2008, 2010; Risi et al., 2010c). We recall here the derivation of this equation and the underlying assumptions.

The isotopic composition R_E of the evaporation flux from the ocean is given by the Craig and Gordon (1965) equation:

$$R_E = \frac{1}{\alpha_K} \cdot \frac{R_{oce}/\alpha_{eq} - RH_s \cdot R_v}{1 - RH_s}, \quad \text{(A1)}$$

where α_K is the kinetic fractionation coefficient, α_{eq} is the liquid-vapor equilibrium fractionation coefficient and R_{oce} is the isotopic ratio of the ocean surface. The relative humidity at the surface, RH_s is the relative humidity of near-surface air at the temperature of the ocean surface T_s:

$$RH_s = RH_a \cdot \frac{q_{sat}(T_a)}{q_{sat}(T_s)}, \quad \text{(A2)}$$

where q_{sat} is the specific humidity at saturation and RH_a and T_a are the relative humidity and temperature of the near-surface air, respectively.

If we assume that (1) the only source of vapor in the boundary layer is the surface evaporation and (2) the sinks of vapor from the boundary layer do not fractionate (i.e. have the composition of the boundary layer, e.g. air flux going out of the boundary layer), then at stationary state $R_v = R_E$. Combined with Eq. (A1), this leads to (Merlivat and Jouzel, 1979):

$$R_v = \frac{R_{oce}}{\alpha_{eq} \cdot (\alpha_K + RH_s \cdot (1 - \alpha_K))}. \quad \text{(A3)}$$

Applying this equation to $H_2^{18}O$, $H_2^{18}O$ and HDO isotopic ratios, it can be shown that d-excess in the boundary layer vapor increases with SST and that d-excess and ^{17}O-excess decrease with RH_s.

Supplementary material related to this article is available online at: http://www.clim-past.net/9/2173/2013/cp-9-2173-2013-supplement.pdf.

Acknowledgements. We thank Boaz Luz, Eugeni Barkan and Ryu Uemura for sharing their ^{17}O-excess data. We thank two anonymous reviewers for their constructive comments. Simulations were performed on the NEC supercomputer of the IDRIS computing center. We acknowledge the FP7 European Project INTRAMIF and the ANR JC project CITRONNIER.

Edited by: A. Paul

The publication of this article is financed by CNRS-INSU.

References

Barkan, E. and Luz, B.: High precision measurements of $^{17}O/^{16}O$ and $^{18}O/^{16}O$ ratios in H_2O, Rapid Commun. Mass Sp., 19, 3737–3742, 2005.

Barkan, E. and Luz, B.: Diffusivity fractionations of $H_2^{16}O/H_2^{17}O$ and $H_2^{16}O/H_2^{18}O$ in air and their implications for isotope hydrology, Rapid Commun. Mass Sp., 21, 2999–3005, 2007.

Barnes, C. and Allison, G.: Tracing of water movement in the unsaturated zone using stable isotopes of hydrogen and oxygen. J. Hydrol, 100, 143–176., 1988.

Barras, V. and Simmonds, I.: Observation and modelling of stable water isotopes as diagnostics of rainfall dynamics over Southeastern Australia, J. Geophys. Res., 114, D23308, doi:10.1029/2009JD012132, 2009.

Bartlein, P. J., Harrison, S. P., Brewer, S., Connor, S., Davis, B. A. S., Gajewski, K., Guiot, J., Harrison-Prentice, T. I., Henderson, A., Peyron, O., Prentice, I. C., Scholze, M., Seppä, H., Shuman, B., Sugita, S., Thompson, R. S., Viau, A. E., Williams, J., Wu, H. , O. P.: Pollen-based continental climate reconstructions at 6 and 21 ka: a global synthesis, Clim. Dynam., 37, 775–802, doi:10.1007/s00382-010-0904-1, 2010.

Bony, S. and Emanuel, K. A.: A parameterization of the cloudiness associated with cumulus convection, evaluation using TOGA COARE data, J. Atmos. Sci., 58, 3158–3183, 2001.

Bony, S., Risi, C., and Vimeux, F.: Influence of convective processes on the isotopic composition (δO^{18} and δD) of precipitation and water vapor in the Tropics, Part 1: radiative-convective equilibrium and TOGA-COARE simulations, J. Geophys. Res., 113, D19305, doi:10.1029/2008JD009942, 2008.

Braconnot, P., Otto-Bliesner, B., Harrison, S., Joussaume, S., Peterchmitt, J.-Y., Abe-Ouchi, A., Crucifix, M., Driesschaert, E., Fichefet, Th., Hewitt, C. D., Kageyama, M., Kitoh, A., Laîné, A., Loutre, M.-F., Marti, O., Merkel, U., Ramstein, G., Valdes, P., Weber, S. L., Yu, Y., and Zhao, Y.: Results of PMIP2 coupled simulations of the Mid-Holocene and Last Glacial Maximum – Part 1: experiments and large-scale features, Clim. Past, 3, 261–277, doi:10.5194/cp-3-261-2007, 2007.

Cappa, C., Hendricks, M., DePaolo, D., and Cohen, R.: Isotopic fractionation of water during re-evaporation, J. Geophys. Res., 108, 4525–4542, 2003.

Ciais, P. and Jouzel, J.: Deuterium and oxygen 18 in precipitation: isotopic model, including cloud processes, J. Geophys. Res., 99, 16793–16803, 1994.

CLIMAP project members: Seasonal reconstructions of the Earth's surface at the last glacial maximum, Geol. Soc. Am., Map Chart Ser. MC-36, 1981.

Craig, H. and Gordon, L. I.: Deuterium and oxygen-18 variations in the ocean and marine atmosphere, Stable Isotope in Oceanographic Studies and Paleotemperatures, edidted by: E. Tongiorgi, 9-130, Pisa: Lab. Geol. Nucl., 1965.

Dansgaard, W: Stable isotopes in precipitation, Tellus, 16, 436–468, 1964.

Delaygue, G.: Relations entre surface océanique et composition isotopique des précipitations antarctiques: simulations pour différents climats, Ph. D. thesis, Université d'Aix-Marseille III, France, 2000.

Franz, P. and Roeckmann, T.: High-precision isotope measurements of h2o, h2o17, h2o18 and delta17o of water vapour in the southern lowermost stratosphere. Atmos. Chem. Physics, 5, 2949–2959, 2005.

Delmotte, M., Masson, V., Jouzel, J., and Morgan, V.: A seasonal deuterium excess signal at Law Dome, coastal Eastern Antarctica: a southern ocean signature, J. Geophys. Res., 105, 7187–7197, 2000.

Dutton, A. L., Wilkinson, B., Welker, J. M., and Lohmann, K. C.: Comparison of river water and precipitation $\delta^{18}O$ across the 48 contiguous United States, Hydrol. Processes, 19, 3551–3572, 2005.

Ehhalt, D. H.: Vertical profiles of hto, hdo, and h2o in the troposphere, NCAR technical note, NCAR-TN-STR-100, 1974.

Ekaykin, A. A., Hondoh, T., Lipenkov, V. Y., and Miyamoto, A.: Post-depositional changes in snow isotope content: preliminary results of laboratory experiments, Clim. Past Discuss., 5, 2239–

2267, 2009.

Ellehoej, M.: Ice-vapor equilibrium fractionation factor experimental investigations and possible impacts on the understanding of the hydrological cycles on Earth and Mars, Ph. D. thesis, University of Copenhagen, Denmark, 2011.

Emanuel, K. A.: A scheme for representing cumulus convection in large-scale models, J. Atmos. Sci., 48, 2313–2329, 1991.

Emanuel, K. A. and Zivkovic-Rothman, M.: Development and evaluation of a convection scheme for use in climate models, J. Atmos. Sci., 56, 1766–1782, 1991.

Farrera, I., Harrison, S. P., Prentice, I. C., Ramstein, G., Guiot, J., Bartlein, P. J., Bonnefille, R., Bush, M., Cramer, W., von Grafenstein, U., Holmgren, K., Hoohiemstra, H., Hope, G., Jolly, D., Lauritzen, S.-E., Ono, Y., Pinot, S., Stute, M., and Yu, G.: Tropical climates at the Last Glacial Maximum: a new synthesis of terrestrial palaeoclimate data, part I: vegetation, lake-levels and geochemistry, Clim. Dynam., 15, 823–856, 1999.

Fekete, B., Gibson, J., Aggarwal, P., and Vorosmarty, C. J.: Application of isotope tracers in continental scale hydrological modeling, J. Hydrol., 330, 444–456, 2006.

Frankenberg, C., Yoshimura, K., Warneke, T., Aben, I., Butz, A., Deutscher, N., Griffith, D., Hase, F., Notholt, J., Schneider, M., Schrijver, H., and Röckmann, T.: Dynamic processes governing lower-tropospheric HDO/H_2O ratios as observed from space and ground, Science, 325, 1374–1377, 2009.

Galewsky, J. and Hurley, J. V.: An advection-condensation model for subtropical water vapor isotopic ratios, J. Geophys. Res., 115, D16115, doi:10.1029/2009JD013651, 2010.

Gat, J. R.: Atmospheric water balance-the isotopic perspective, Hydrol. Process., 14, 1357–1369, 2000.

Gat, J. R. and Matsui, E.: Atmospheric water balance in the Amazon Basin: an isotopic evapotranspiration model, J. Geophys. Res., 96, 13179–13188, 1991.

Gat, J. R., Shemesh, A., Tziperman, E., Hecht, A., Georgopoulos, D., and Basturk, O.: The stable water isotope composition of waters in the Eastern Mediterranean Sea, J. Geophys. Res., 101, 6441–6451, 1996.

Gates, W. L.: AMIP: the atmospheric model intercomparison project, B. Am. Meteor. Soc., 73, 1962–1970, 1992.

Gibson, J. J., Edwards, T. W. D., Birks, S. J., Amour, N. A. S., Buhay, W. M., McEachern, P., Wolfe, B. B., and Peters1, D. L.: Progress in isotope tracer hydrology in Canada, Hydrol. Processes, 19, 303–327, 2005.

Gurney, S. D. and Lawrence, D. S. L.: Seasonal trends in the stable isotopic composition of snow and meltwater runoff in a subarctic catchment at okstindan, Nord. Hydrol., 35, 119–137, 2004.

Hendricks, M., DePaolo, D., and Cohen, R.: Space and time variation of $\delta^{18}O$ and δD: can paelotemperatures be estimated from ice cores?, Glob. Geochem. Cy., 14, 851–861, 2000.

Hoffmann, G., Werner, M., and Heimann, M.: Water isotope module of the ECHAM atmospheric general circulation model: a study on timescales from days to several years, J. Geophys. Res., 103, 16871–16896, 1991.

Hourdin, F. and Armengaud, A.: The use of finite-volume methods for atmospheric advection of trace species, Part I: test of various formulations in a general circulation model, Mon. Weather Rev., 127, 822–837, 1999.

Hourdin, F., Musat, I., Bony, S., Braconnot, P., Codron, F., Dufresne, J.-L., Fairhead, L., Filiberti, M.-A., Friedlingstein, P., Grandpeix, J.-Y., Krinner, G., Levan, P., Li, Z.-X., and Lott, F.: The LMDZ4 general circulation model: climate performance and sensitivity to parametrized physics with emphasis on tropical convection, Clim. Dynam., 27, 787–813, 2006.

Johnsen, S., Dansgaard, W., Clausen, H., and Langway, J. C.: Oxygen isotope profiles through the Antarctic and Greenland ice sheets, Nature, 235, 429–434, 1972.

Johnson, D. G., Jucks, K. W., Traub, W. A., and Chance, K. V.: Isotopic composition of stratospheric water vapor: implications for transport, J. Geophys. Res., 106, 12219–12226, 2001.

Joussaume, S. and Taylor, K. E.: Status of the paleoclimate modeling intercomparison project, in: Proceedings of the first international AMIP scientific conference, WCRP-92, Monterey, 15–19 May 1995, USA, 425–430, 1995.

Jouzel, J.: Isotopes in cloud physics: Multiphase and multistage condensation processes. Elsevier, 1986.

Jouzel, J.: Water stable isotopes: atmospheric composition and applications in polar ice core studies, Treatise on Geochemistry, 4, 213–243, 2003.

Jouzel, J. and Koster, R. D.: A reconsideration of the initial conditions used for stable water isotope models, J. Geophys. Res., 101, 22933–22938, 1996.

Jouzel, J. and Merlivat, L.: Deuterium and oxygen 18 in precipitation: modeling of the isotopic effects during snow formation, J. Geophys. Res., 89, 11749–11757, doi:10.1029/JD089iD07p11749, 1984.

Jouzel, J., Merlivat, L., and Lorius, C.: Deuterium excess in an East Antarctic ice core suggests higher relative humidity at the oceanic surface during the last glacial maximum, Nature, 299, 688–691, 1982.

Kendall, C. and Coplen, T. B.: Distribution of oxygen-18 and deuterium in river waters across the United States, Hydrol. Process., 15, 1363–1393, 2001.

Krinner, G., Viovy, N., de Noblet-Ducoudre, N., Ogee, J., Polcher, J., Friedlingstein, P., Ciais, P., Sitch, S., and Prentice, I. C.: A dynamic global vegetation model for studies of the coupled atmosphere-biosphere system, Glob. Biogeochem. Cycles, 19, GB1015, doi:10.1029/2003GB002199, 2005.

Lai, C.-T. and Ehleringer, J. R.: Deuterium excess reveals diurnal sources of water vapor in forest air, Oecologia, 165, 213–223, doi:10.1007/s00442-010-1721-2, 2011..

Landais, A., Barkan, E., and Luz, B: The triple isotopic composition of oxygen in leaf water, Geochim. Cosmochim. Ac., 70, 4105–4115, 2006.

Landais, A., Barkan, E., and Luz, B.: Record of δ^{18}O and ^{17}O-excess in ice from Vostock Antarctica during the last 150 000 years, Geophys. Res. Lett., 35, L02709, doi:10.1029/2007GL032096, 2008.

Landais, A., Risi, C., Bony, S., Vimeux, F., Descroix, L., Falourd, S., and Bouygues, A.: Combined measurements of ^{17}O-excess and d-excess in African monsoon precipitation: implications for evaluating convective parameterizations, Earth Planet. Sci. Lett., 298, 104–112, 2010.

Landais, A., Ekaykin, A., Barkan, E., Winkler, R., and Luz, B.: Seasonal variations of ^{17}O-excess and d-excess in snow precipitation at Vostok station, East Antarctica, J. Glaciol., 58, 725–733, doi:10.3189/2012JoG11J237, 2012a.

Landais, A., Steen-Larsen, H.-C., Guillevic, M., Masson-Delmotte, V., Vinther, B., and Winkler, R.: Triple isotopic

composition of oxygen in surface snow and water vapor at NEEM (Greenland), Geochim. Cosmochim. Ac., 77, 304–316, 2012b.

Lawrence, J. R., Gedzelman, S. D., Dexheimer, D., Cho, H.-K., Carrie, G. D., Gasparini, R., Anderson, C. R., Bowman, K. P., and Biggerstaff, M. I.: Stable isotopic composition of water vapor in the tropics, J. Geophys. Res., 109, D06115, doi:10.1029/2003JD004046, 2004.

Lee, J.-E. and Fung, I.: "Amount effect" of water isotopes and quantitative analysis of post-condensation processes, Hydrol. Process., 22, 1–8, 2008.

Lee, J.-E., Fung, I., DePaolo, D. J., and Otto-Bliesner, B.: Water isotopes during the Last Glacial Maximum: new general circulation model calculations, J. Geophys. Res., 113, D19109, doi:10.1029/2008JD009859, 2008.

Lee, J., Feng, X., Faiia, A. M., Posmentier, E. S., Kirchner, J. W., Osterhuber, R., and Taylor, S.: (2010). Isotopic evolution of a seasonal snowcover and its melt by isotopic exchange between liquid water and ice. Chemical Geology, 270, 126–134, doi:10.1016/j.chemgeo.2009.11.011, 2010.

Letreut, H. and Li, Z.-X.: Sensitivity of an atmospheric general circulation model to prescribed sst changes: feedback effects associated with the simulation of cloud optical properties. Cli, 5, 175–187, 1991.

Lorius, C., Merlivat, L., Jouzel, J., and Pourchet, M.: A 30000 yr isotope climatic record from Antarctic ice, Nature, 280, 644–648, 1979.

Luz, B. and Barkan, E.: Variations of ^{17}O/^{16}O and ^{18}O/^{16}O in meteoric waters, Geochim. Cosmochim. Ac., 74, 6276–6286, 2010.

Luz, B., Barkan, E., Yam, R., and Shemesh, A.: Fractionation of oxygen and hydrogen isotopes in evaporating water, Geochim. Cosmochim. Ac., 73, 6697–6703, 2009.

Majoube, M.: Fractionnement en ^{18}O entre la glace et la vapeur d'eau, J. Chim. Phys., 68, 625–636, 1971a.

Majoube, M.: Fractionnement en Oxygène 18 et en Deutérium entre l'eau et sa vapeur, J. Chim. Phys., 10, 1423–1436, 1971b.

MARGO project members: Constraints on the magnitude and patterns of ocean cooling at the Last Glacial Maximum, Nat. Geosci., 2, 127–132, 2008.

Marti, O., Braconnot, P., Bellier, J., Benshila, R., Bony, S., Brockmann, P., Cdule, P., Caubel, A., Denvil, S., Dufresne, J.-L., Fairhead, L., Filiberti, M.-A., Foujols, M.-A., Fichefer, T., Friedlingstein, P., Grandpeix, J.-Y., Hourdin, F., Krinner, G., Lévy, C., Madec, G., Musat, I., de Noblet, N., Polcher, J., and Tanlandier, C.: The new IPSL climate system model: IPSL-CM4, Technical report, IPSL, France, 2005.

Masson-Delmotte, V., Jouzel, J., Landais, A., Stievenard, M., Johnsen, S. J., White, J. W. C., Werner, M., Sveinbjornsdottir, A., and Fuhrer, K.: GRIP Deuterium excess reveals rapid and orbital-scale changes in Greenland moisture origin, Science, 309, 118–121, 2005.

Masson-Delmotte, V., Hou, S., Ekaykin, A., Jouzel, J., Aristarain, A., Bernardo, R. T., Bromwhich, D., Cattani, O., Delmotte, M., Falourd, S., Frezzotti, M., Gallée, H., Genoni, L., Isaksson, E., Landais, A., Helsen, M., Hoffmann, G., Lopez, J., Morgan, V., Motoyama, H., Noone, D., Oerter, H., Petit, J., Royer, A., Uemura, R., Schmidt, G., Schlosser, E., Simes, J., Steig, E., Stenni, B., Stievenard, M., van den Broeke, M., van de Wal, R., van den Berg, W.-J., Vimeux, F., and White, J.: A review of Antarctic surface snow isotopic composition: observations, atmospheric circulation and isotopic modelling, J. Climate, 21, 3359–3387, 2008.

Masson-Delmotte, V., Braconnot, P., Hoffmann, G., Jouzel, J., Kageyama, M., Landais, A., Lejeune, Q., Risi, C., Sime, L., Sjolte, J., Swingedouw, D., and Vinther, B.: Sensitivity of interglacial Greenland temperature and δ^{18}O: ice core data, orbital and increased CO_2 climate simulations, Clim. Past, 7, 1041–1059, doi:10.5194/cp-7-1041-2011, 2011.

Meehl, G. A., Covey, K., Delworth, T., Latif, M., McAvaney, B., Mitchell, J. F. B., Stouffer, R. J., and Taylor, K.: The WCRP CMIP3 multimodel dataset: a new era in climate change research, B. Am. Meteor. Soc., 7, 1383–1394, 2007.

Merlivat, L. and Jouzel, J.: Global climatic interpretation of the Deuterium-Oxygen 18 relationship for precipitation, J. Geophys. Res., 84, 5029–5332, 1979.

Merlivat, L. and Nief, G.: Fractionnement isotopique lors des changements d'états solide-vapeur et liquide-vapeur de l'eau à des températures inférieures à 0C, Tellus, 19, 122–127, 1967.

Noone, D.: The influence of midlatitude and tropical overturning circulation on the isotopic composition of atmospheric water vapor and Antarctic precipitation, J. Geophys. Res., 113, D04102, doi:10.1029/2007JD008892, 2008.

Peltier, W. R.: Ice age paleotopography, Science, 265, 195–201, 1994.

Polcher, J.: Les processus de surface à l'échelle globale et leurs interactions avec l'atmosphère, in: Thèse d'habilitation à diriger des recherches, Université Paris 6, 2003.

Risi, C., Bony, S., and Vimeux, F.: Influence of convective processes on the isotopic composition (^{18}O and D) of precipitation and water vapor in the Tropics, Part 2: Physical interpretation of the amount effect, J. Geophys. Res., 113, D19306, doi:10.1029/2008JD009943, 2008a.

Risi, C., Bony, S., Vimeux, F., Descroix, L., Ibrahim, B., Lebreton, E., Mamadou, I., and Sultan, B.: What controls the isotopic composition of the African monsoon precipitation? Insights from event-based precipitation collected during the 2006 AMMA campaign, Geophys. Res. Lett., 35, doi:10.1029/2008GL035920, 2008b.

Risi, C.: *Les isotopes stables de l'eau: applications à l'étude du cycle de l'eau et des variations du climat*, PhD thesis, Université Pierre et Marie Curie, 2009.

Risi, C., Bony, S., Vimeux, F., Chong, M., and Descroix, L.: Evolution of the water stable isotopic composition of the rain sampled along Sahelian squall lines, Quart. J. Roy. Meteor. Soc., 136, 227–242, 2010a.

Risi, C., Bony, S., Vimeux, F., and Jouzel, J.: Water stable isotopes in the LMDZ4 general circulation model: model evaluation for present day and past climates and applications to climatic interpretation of tropical isotopic records, J. Geophys. Res., 115, D12118, doi:10.1029/2009JD013255, 2010b.

Risi, C., Landais, A., Bony, S., Masson-Delmotte, V., Jouzel, J., and Vimeux, F.: Understanding the ^{17}O-excess glacial-interglacial variations in Vostok precipitation, J. Geophys. Res, 115, D10112, doi:10.1029/2008JD011535, 2010c.

Risi, C., Noone, D., Worden, J., Frankenberg, C., Stiller, G., Kiefer, M., Funke, B., Walker, K., Bernath, P., Schneider, M., Wunch, D., Sherlock, V., Deutscher, N., Griffith, D., Wernberg, P., Bony, S., Lee, J., Brown, D., Uemura, R., and Sturm, C.: Process-

evaluation of tropical and subtropical tropospheric humidity simulated by general circulation models using water vapor isotopic observations. Part 2: an isotopic diagnostic of the mid and upper tropospheric moist bias, J. Geophy. Res., 117, D05304, 2012.

Rozanski, K., Araguas-Araguas, L., and Gonfiantini, R.: Isotopic patterns in modern global precipitation, Geophysical Monographs Series, AGU, Climate Change in Continental Isotopic records, vol. 78, edited by: Swart, P. K., Lohwan, K. L., McKenzie, J. A., and Savin, S., 1–36, AGU, Washington, D. C., doi::10.1029/GM078p00011993, 1993.

Sayres, D. S., Pfister, L., Hanisco, T. F., Moyer, E. J., Smith, J. B., Clair, J. M. S., O'Brien, A. S., Witinski, M. F., Legg, M., and Anderson, J. G.: Influence of convection on the water isotopic composition of the tropical tropopause layer and tropical stratosphere, J. Geophys. Res., 11, D00J20, doi:10.1029/2009JD013100, 2010.

Schoenemann, S. W., Schauer, A. J., and Steig, E. J.: Measurement of SLAP2 and GISP d^{17}O and proposed VSMOWSLAP normalization for d^{17}O and ^{17}Oexcess, Rapid Commun. Mass Spectrom., 27, 582–590, 2013.

Sherwood, S. C.: Maintenance of the free tropospheric tropical water vapor distribution, part II: simulation of large-scale advection, J. Climate, 11, 2919–2934, 1996.

Sobel, A. H. and Bretherton, C. S.: Modeling tropical precipitation in a single column, J. Climate, 13, 4378–4392, 2000.

Sodemann, H., Masson-Delmotte, V., Schwierz, C., Vinther, B. M., and Wernli, H.: Interannual variability of Greenland winter precipitation sources: 2. Effects of North Atlantic Oscillation variability on stable isotopes in precipitation, J. Geophys. Res., 113, D12, doi:10.1029/2007JD009416, 2008.

Steen-Larsen, H.-C., Johnsen, S., Masson-Delmotte, V., Stenni, B., Risi, C., Sodemann, H., Balslev-Clausen, D., Blunier, T., Dahl-Jensen, D., Ellehoej, M., Falourd, S., Gkinis, V., Grindsted, A., Jouzel, J., Popp, T., Sheldon, S., Simonsen, S., Sjolte, J., Steffensen, J., Sperlich, P., Sveinbjornsdottir, A., Vinther, B., and White, J.: Continuous monitoring of summer surface water vapour isotopic composition above the greenland ice sheet, Atmos. Chem. Phys., 13, 4815–4828, doi:10.5194/acp-13-4815-2013, 2013.

Stenni, B., Masson-Delmotte, V., Johnsen, S., Jouzel, J., Longinelli, A., Monnin, E., Röthlisberger, R., and Selmo, E.: An oceanic cold reversal during the last deglaciation, Science, 293, 2074–2077, 2001.

Stenni, B., Jouzel, J., Masson-Delmotte, V., Röthlisberger, R., Castellano, E., Cattani, O., Falourd, S., Johnsen, S., Longinelli, A., Sachs, J., Selmo, E., Souchez, R., Steffensen, J., and Udisti, R.: A late-glacial high-resolution site and source temperature record derived from the epica dome c isotope records (East Antarctica), Earth Planet. Sci. Lett., 217, 183–195, 2004.

Stewart, M. K.: Stable isotope fractionation due to evaporation and isotopic exchange of falling waterdrops: applications to atmospheric processes and evaporation of lakes, J. Geophys. Res., 80, 1133–1146, 1975.

Taylor, S., F. X. H. K. J. W. O. R. K. B. and Renshaw, C. E.: Isotopic evolution of a seasonal snowpack and its melt, Water Resour. Res., 37, 759–769, 2001.

Uemura, R., Matsui, Y., Yoshimura, K., Motoyama, H., and Yoshida, N.: Evidence of deuterium-excess in water vapour as an indicator of ocean surface conditions, J. Geophys. Res., 113, D19114, doi:10.1029/2008JD010209, 2008.

Uemura, R., Barkan, E., Abe, O., and Luz, B.: Triple isotope composition of oxygen in atmospheric water vapor, Geophy. Res. Lett., 37, L04402, doi:10.1029/2009GL041960, 2010.

Uppala, S., Kallberg, P., Simmons, A., Andrae, U., da Costa Bechtold, V., Fiorino, M., Gibson, J., Haseler, J., Hernandez, A., Kelly, G., Li, X., Onogi, K., Saarinen, S., Sokka, N., Allan, R., Andersson, E., Arpe, K., Balmaseda, M., Beljaars, A., van de Berg, L., Bidlot, J., Bormann, N., Caires, S., Chevallier, F., Dethof, A., Dragosavac, M., Fisher, M., Fuentes, M., Hagemann, S., Holm, E., Hoskins, B., Isaksen, L., Janssen, P., Jenne, R., McNally, A., Mahfouf, J.-F., Morcrette, J.-J., Rayner, N., Saunders, R., Simon, P., Sterl, A., Trenberth, K., Untch, A., Vasiljevic, D., Viterbo, P., and Woollen, J.: The ERA-40 re-analysis, Q. J. Roy. Meteor. Soc., 131, 2961–3012, 2005.

Van Hook, A.: Vapor pressures of the isotopic waters and ices. J. Phys. Chem., 1234, 1968.

Van Leer, B.: Towards the ultimate conservative difference scheme, IV: a new approach to numerical convection, J. Comput. Phys., 23, 276–299, 1977.

Vimeux, F., Masson, V., Jouzel, J., Stievenard, M., and Petit, J. R.: Glacial-interglacial changes in ocean surface conditions in the Southern Hemisphere, Nature, 398, 410–413, 1999.

Vimeux, F., Masson, V., Delaygue, G., Jouzel, J., Petit, J. R., and Stievenard, M.: A 420 000 year deuterium excess record from East Antarctica: information on past changes in the origin of precipitation at Vostok, J. Geophys. Res., 106, 31863–31873, 2001a.

Vimeux, F., Masson, V., Jouzel, J., Petit, J.-R., Steig, E., Stievenard, M., Vaikmae, R., and White, J. W.: Holocene hydrological cycle changes in the Southern Hemisphere documented in East antarctic deuterium excess records, Clim. Dynam., 17, 503–513, 2001b.

Vimeux, F., Cuffey, K., and Jouzel, J.: New insights into Southern Hemisphere temperature changes from Vostok ice cores using deuterium excess correction, Earth Planet. Sci. Lett., 203, 829–843, 2002.

Vimeux, F., Gallaire, R., Bony, S., Hoffmann, G., and Chiang, J. C. H.: What are the climate controls on deltaD in precipitation in the Zongo Valley (Bolivia)? Implications for the Illimani ice core interpretation, Earth Planet. Sci. Lett., 240, 205–220, 2005.

Washburn, E. and Smith, E.: The isotopie fractionation of water by physiological processes, Science, 79, 188–189, 1934.

Welp, L., Lee, W., Griffis, T. J., Wen, X.-F., Xiao, W., Li, S., Sun, X., Hu, Z., Val Martin, M., and Huang, J.: A meta-analysis of water vapor deuterium-excess in the midlatitude atmospheric surface layer, Glob. Biogeochem. Cycles, 26, GB3021, doi:10.1029/2011GB004246, 2012.

Wen, X.-F., Zhang, S.-C., Sun, X.-M., Yu, G.-R., and Lee, X.: Water vapor and precipitation isotope ratios in Beijing, China. J. Geophys. Res, 115, D01103, doi:10.1029/2009JD012408, 2010.

Werner, M., Heimann, M., and Hoffmann, G.: Isotopic composition and origin of polar precipitation in present and glacial climate simulations, Tellus B, 53, 53–71, 2001.

Winkler, R., Landais, A., Sodemann, H., Dümbgen, L., Prié, F., Masson-Delmotte, V., Stenni, B., and Jouzel, J.: Deglaciation records of ^{17}O-excess in East Antarctica: reliable reconstruction of oceanic normalized relative humidity from coastal sites, Clim.

Past, 8, 1–16, doi:10.5194/cp-8-1-2012, 2012.
Winkler, R., Landais, Risi, C., A., Baroni, M., Ekaykin, A., Jouzel, J., Petit, J. R., Prie, F., Minster, B., Falourd, S.:Interannual variation of water isotopologues at Vostok indicates a contribution from stratospheric water vapor. Proc. Natl. Acad. Ssi., accepted, doi:10.1073/pnas.1215209110, 2013.
Worden, J., Noone, D., and Bowman, K.: Importance of rain evaporation and continental convection in the tropical water cycle, Nature, 445, 528–532, 2007.
Zahn, A., Franz, P., Bechtel, C., Grooß, J.-U., and Röckmann, T.: Modelling the budget of middle atmospheric water vapour isotopes, Atmos. Chem. Phys., 6, 2073–2090, doi:10.5194/acp-6-2073-2006, 2006.